



# Estimating Bedload From Suspended Load and Water Discharge in Sand Bed Rivers

T. C. Ashley<sup>1\*</sup>, B. McElroy<sup>1</sup>, D. Buscombe<sup>2</sup>, P. E. Grams<sup>3</sup>, and M. Kaplinski<sup>2</sup>

<sup>1</sup>Department of Geology and Geophysics, University of Wyoming, Laramie, WY

<sup>2</sup>School of Earth and Sustainability, Northern Arizona University, Geosciences Division, Flagstaff, AZ

<sup>3</sup>US Geological Survey, Southwest Biological Science Center, Grand Canyon Monitoring and Research Center, Flagstaff, AZ

## Key Points:

- Bedload flux is predicted from variables that are measured at acoustic suspended sediment monitoring stations.
- Bayesian modeling extends the utility of this approach to a wide range of conditions and rivers.
- Predicted bedload flux provides an indicator of short-term sediment supply enrichment and depletion.

\*1000 E. University Ave, Laramie, WY, USA

Corresponding author: Thomas Ashley, tashley3@uwy.edu

15      **Abstract**

16      Estimates of fluvial sediment discharge from in situ instruments are an important com-  
 17      ponent of large-scale sediment budgets that track long-term geomorphic change. Sus-  
 18      pended sediment load can be reliably estimated using acoustic or physical sampling tech-  
 19      niques; however, bedload is difficult to measure directly and can consequently be one of  
 20      the largest sources of uncertainty in estimates of total load. We propose a physically-  
 21      informed predictive empirical model for bedload sand flux as a function of variables that  
 22      are measured using existing acoustic or physical sampling techniques. This model depends  
 23      on the assumption that concentration and grain size in suspension are in equilibrium with  
 24      reach-averaged boundary conditions. Bayesian inference is used to fit model parameters  
 25      to data from eight sand-bed rivers and to simulate bedload flux over the available gage  
 26      record at one site on the Colorado River in Grand Canyon National Park. We find that the  
 27      cumulative bedload flux during the nine year period from 2008 to 2016 was 5% of the cu-  
 28      mulative suspended sand load; however, instantaneous bedload flux ranged from as little as  
 29      1% of instantaneous suspended sand load to as much as 75% of instantaneous suspended  
 30      sand load due to fluctuations in flow strength and sediment supply. Changes in bedload  
 31      flux at a constant discharge are indicative of short-term sediment supply enrichment and  
 32      depletion. Long-term average bedload flux cannot be expected to remain constant in the  
 33      future as the river adjusts to changes in sediment runoff and the dam-regulated discharge  
 34      regime.

35      **1 Introduction**

36      Estimates of fluvial sediment load provide an important tool for quantifying large-  
 37      scale geomorphic change. In a wide range of environments, suspended sediment load can  
 38      be accurately constrained using acoustic surrogates for sediment concentration [Topping  
 39      et al., 2004; Topping & Wright, 2016], enabling low-cost measurement of suspended load  
 40      at high temporal resolutions over multi-year timescales [Dean et al., 2016; Grams et al.,  
 41      2013, 2018]. However, acoustic estimates of flux depend on assumptions about the verti-  
 42      cal concentration distribution that are reasonable if not strictly valid in the interior of the  
 43      flow [Gray & Gartner, 2010] but that become increasingly dubious in the near-bed region.  
 44      Bedload may vary significantly with respect to suspended sediment load due to changes in  
 45      Rouse conditions [van Rijn, 1984].

46      Existing procedures for measuring bedload separately from suspended load in sand-  
 47      bedded rivers [Gray et al., 2010; Holmes, 2019] are incompatible with the goals and lim-  
 48      itations of long-term monitoring. Direct physical sampling is costly and can be inaccu-  
 49      rate in large rivers due to undersampling [Pitlick, 1988], and existing predictive bedload  
 50      transport models that might be used in lieu of direct measurements (e.g. Wong & Parker  
 51      [2006]) generally require, at minimum, an estimate of the skin friction component of bed  
 52      shear stress, which in turn necessitates additional measurements or models each subject to  
 53      their own logistical limitations and uncertainty. Sediment budgets therefore rely on simpli-  
 54      fied treatments of bedload flux that can introduce large persistent biases to estimates of to-  
 55      tal bed material load. For example, bedload is typically estimated either as a constant frac-  
 56      tion of suspended load [Grams et al., 2013], a power-law function of water discharge (i.e.  
 57      a rating curve) [Ellison et al., 2016], or ignored [Wright et al., 2010]. This is problematic  
 58      because bedload flux can be a substantial fraction of total load in suspension-dominated  
 59      rivers, particularly at low flow conditions [Turowski et al., 2010]; bedload flux can vary  
 60      relative to suspended load due changes in suspension conditions, and it can vary with re-  
 61      spect to a fixed water discharge due to changes in bed material composition and channel  
 62      geometry [Topping et al., 2000a,b].

63      The purpose of this paper is to provide a reliable means for estimating bedload flux  
 64      in sand-bed rivers when suspended sediment information is available. The rationale behind  
 65      our approach is that bedload and suspended load are mutually determined by the same

causal boundary conditions at the reach-averaged scale. As a result, measured changes in concentration and grain size in suspension can be used to deduce changes in these boundary conditions and estimate bedload flux. This concept was first proposed by *Rubin & Topping* [2001] and underlies an empirical model that expresses bedload flux per unit channel width as a function of unit water discharge, suspended sand concentration, and suspended sand diameter.

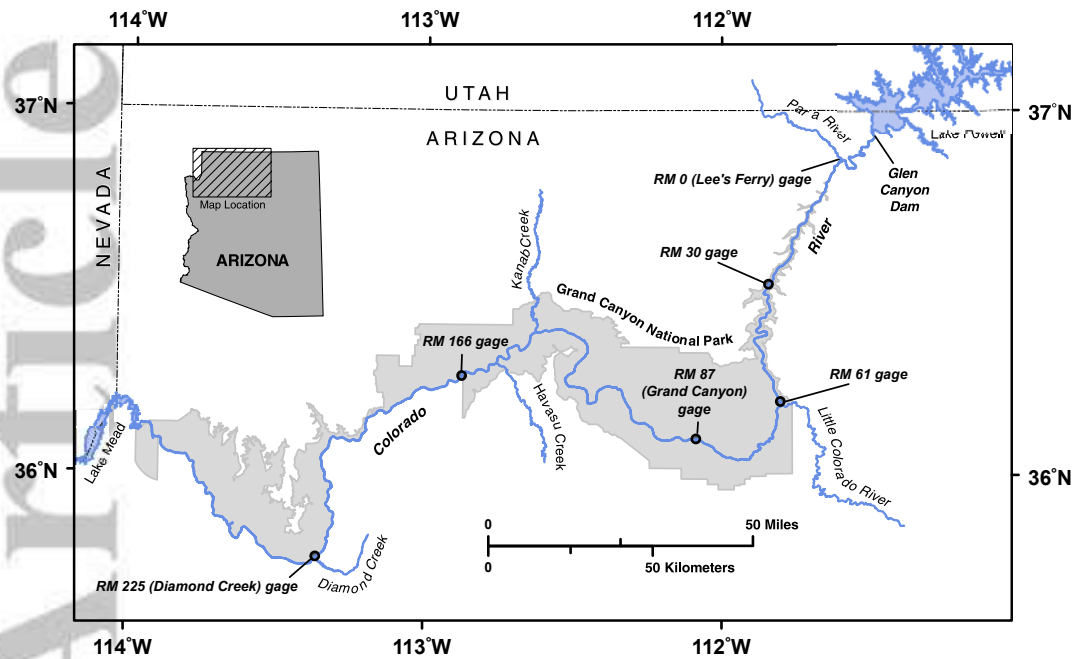
Our primary goal is to estimate bedload flux from gage data and propagate uncertainty through estimates of cumulative load. This is accomplished using Bayesian inference, which provides a convenient framework for quantifying uncertainty in sediment transport parameters using numerical Markov chain Monte-Carlo (MCMC) methods [*Schmelter et al.*, 2011; *Schmelter & Stevens*, 2012; *Schmelter et al.*, 2015]. Moreover, Bayesian techniques implemented in the MCMC framework enable rigorous propagation of uncertainty through individual estimates of sediment load and time-integrated mass balance calculations [*Schmelter et al.*, 2012].

Our model can be applied in any sand-bedded river and does not require site-specific calibration. However, our analysis reveals that predictions may be biased on a site-specific basis such that greater predictive accuracy is achieved when the model is fit using only data from one site. This is particularly important when computing sediment budgets because error associated with model bias accumulates over time [*Grams et al.*, 2013]. Unfortunately, site-specific data are not always available; in order to meet the varying needs of different applications, we present three modeling approaches that utilize historical data from seven rivers reported by *Toffaleti* [1968] to varying degrees. The first approach involves pooling all data to estimate model parameters and is acceptable for obtaining single estimates of bedload flux at sites where no direct observations are available. The second approach utilizes only data from the site of interest, and is suitable when extensive site-specific data are available. The third approach involves a hierarchical modeling framework [*Gelman et al.*, 1995; *Christensen et al.*, 2011] that optimizes use of limited site-specific data by using sites with many observations to inform prediction at sites with relatively few observations. Application of all three approaches is demonstrated at one sediment monitoring station on the Colorado river. The statistical procedure presented here ultimately provides a convenient method for tracking changes in bedload flux driven by flow strength and sediment supply limitation over timescales ranging from days to years.

## 2 Colorado River sediment monitoring

On the Colorado River in Grand Canyon National Park, flux-based sediment budgets inform flow regulation protocols aimed at minimizing the downstream impact of Glen Canyon Dam. The primary management objective is the reversal of long-term depletion of alluvial sand deposits, especially emergent deposits known as eddy sand bars, through the use of controlled floods [*Topping et al.*, 2010; *Wright & Kaplinski*, 2011; *Grams et al.*, 2015]. However, the range of available management solutions is limited; this objective must be accomplished without compromising other economic [*Ingram et al.*, 1991] and ecological [*Minckley*, 1991] objectives. Designing such a protocol requires a detailed understanding of the dynamics of flow and sediment transport through the canyon.

In the dam-regulated Colorado River, the upstream sediment supply is completely independent from water discharge. Undammed tributaries comprise the only resupply of alluvial material to the post-dam river, while the hydrograph is determined by clear water releases from Lake Powell [*Andrews*, 1991; *Topping et al.*, 2000a; *Rubin et al.*, 2002]. Sediment supply and flow fluctuations cause complex morphodynamic interactions as the channel adjusts to accommodate pulses of sediment under the imposed discharge regime. Confinement by bedrock and bouldery debris fans also limits the extent to which flow can modify local slope and hydraulic geometry. As a result, antecedent sedimentary and morphological conditions are as important as water discharge in regulating instantaneous sedi-



139 **Figure 1.** Map of the Colorado River in Grand Canyon National Park, after Grams *et al.* [2013]). Data used  
140 in this study come from the reach adjacent to the Diamond Creek gage located at river mile 225.

117 movement transport [Rubin & Topping, 2001]. This condition, known as “supply limitation,” is  
118 common in natural rivers, but is particularly pronounced on the Colorado River and other  
119 dammed rivers due to artificial flow regulation and sediment starvation [Dolan *et al.*, 1974;  
120 Schmidt & Graf, 1990].

121 Modeling the dynamics of alluvial deposits in supply-limited systems requires sub-  
122 stantial physical simplifications and empiricism (e.g. Wright *et al.* [2010]). Changes in  
123 stored sediment mass estimated from spatial gradients in sediment flux are a useful metric  
124 for evaluating the effects of past flow regimes and for testing predictive models that can  
125 be used to determine best-practice scenarios for the future. The canyon is divided into five  
126 sediment budget reaches, each bounded by monitoring stations on the main stem and ma-  
127 jor tributaries that estimate total sand load every fifteen minutes (Figure 1). At the time  
128 of writing, these records comprise over a decade of almost uninterrupted suspended sedi-  
129 ment data that can be used to quantify morphodynamic trends over a range of timescales:  
130 multi-year trends indicate regime-scale adjustment while short-term variability reflects the  
131 transient response to individual or seasonal perturbations in flow strength and sediment  
132 supply. Data are available online at [https://www.gcmrc.gov/discharge\\_qw\\_sediment/](https://www.gcmrc.gov/discharge_qw_sediment/).

133 Bedload flux is perhaps the largest source of uncertainty in estimates of total sedi-  
134 ment load. At the time of writing, bedload is estimated at all monitoring sites on the Col-  
135 orado River as a constant 5% of suspended load based on a single set of concurrent mea-  
136 surements of bedload and suspended load [Rubin *et al.*, 2001]. Presently, we aim test this  
137 assumption at one site (Figure 2), and reduce bias in estimates of total load by developing  
138 and applying a robust statistical methodology for estimating bedload flux from gage data.

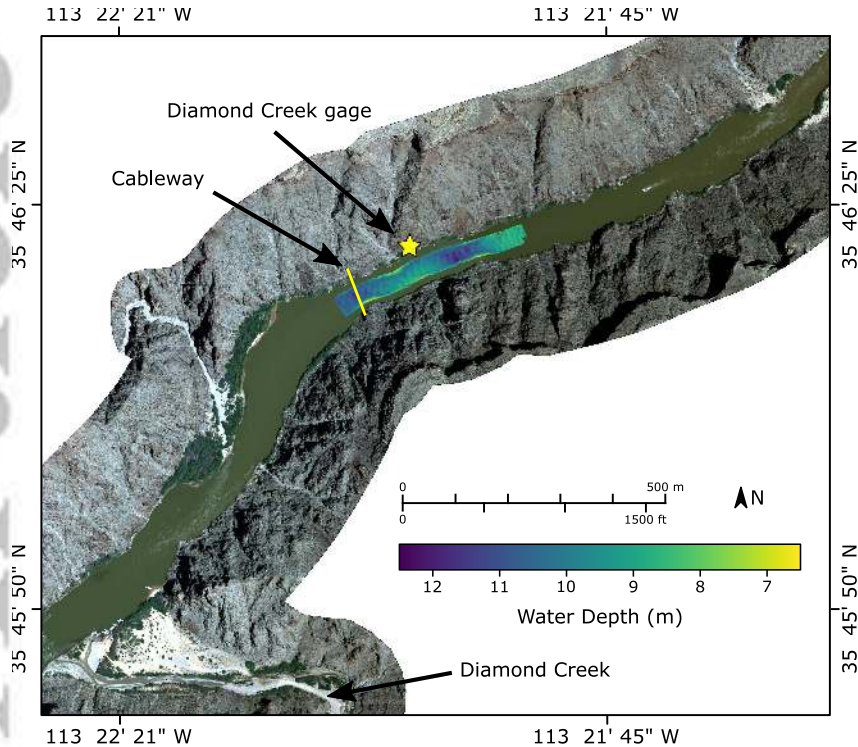


**Figure 2.** Aerial view of the Diamond Creek study site. One survey of water depth is plotted, illustrating the extent of the sonar mapping area.

### 3 Methods and data

#### 3.1 Modeling approach

The goal of this paper is to predict total mass bedload flux,  $Q_b$  [ $MT^{-1}$ ], from measurements of water discharge, suspended sand concentration, and suspended sand diameter. To this end, we adopt an empirical power-law equation for bedload flux per unit width  $q_b$  [ $MT^{-1}L^{-1}$ ] given by:

$$q_b = Ae^{\beta_0} q_w^{\beta_1} C_s^{\beta_2} D_s^{\beta_3}. \quad (1)$$

Here,  $q_w$  [ $L^2/T$ ] is the average volumetric water discharge per unit width equal to  $Q_w/W$ , where  $Q_w$  [ $L^3/T$ ] is the total volumetric water discharge and  $W$  [ $L$ ] is the surface width of the channel.  $C_s$  [ $L/L$ ] is the discharge-averaged suspended sand concentration,  $D_s$  [ $L$ ] is median diameter of suspended sand and  $A$  is a dimensional coefficient expressed in terms of fixed reference values for each variable (denoted by the subscript 0) as  $A = q_{b0}/q_{w0}^{\beta_1} C_{s0}^{\beta_2} D_{s0}^{\beta_3}$ . Finally,  $\beta_0$  is an intercept term that is equal to 0 if reference values are chosen so that  $q_b = q_{b0}$  when  $q_w = q_{w0}$ ,  $C_s = C_{s0}$ , and  $D_s = D_{s0}$ .

Equation (1) is purely empirical; however, we consider the form of this expression in the context of existing theory to (1) facilitate qualitative interpretation of our results and (2) support the notion that in-sample fit will extend to out-of-sample predictive accuracy. Forward models for equilibrium sediment transport [Einstein, 1950; McLean, 1992; Molinas & Wu, 2002; Wright & Parker, 2004] encompass the physical interactions that are relevant to this objective, and generally involve several computational steps that incorporate various physical and empirical expressions. As an example Wright & Parker [2004] proposed a computational procedure for estimating  $C_s$ ,  $D_s$ , and the Shields' stress due to skin friction  $\tau_{*s}$  (among other variables) from specified reach-average boundary conditions, which are  $q_w$ , slope  $S$  [ $L/L$ ], and bed material grain size  $D_b$  [ $L$ ]. Bedload flux can

be computed from  $\tau_{*s}$  using an empirical bedload transport formula [e.g. *Wong & Parker*, 2006]. Additional relevant physical parameters that must be specified are often assumed to be constants. These are gravitational acceleration  $g$  [ $L/T^2$ ], the kinematic viscosity of water  $\nu$  [ $L^2/T$ ], and the densities of sediment  $\rho_s$  [ $M/L^3$ ] and water  $\rho_w$  [ $M/L^3$ ]. In summary, this model approximates three unknown physical equations of the following functional form:

$$q_b = f(q_w, S, D_b, \rho_s, \rho_w, g, \nu) \quad (2)$$

$$C_s = f(q_w, S, D_b, \rho_s, \rho_w, g, \nu) \quad (3)$$

$$D_s = f(q_w, S, D_b, \rho_s, \rho_w, g, \nu). \quad (4)$$

Each forward equation has eight variables (seven predictor variables and one response variable) and three physical dimensions, and can therefore be reduced to five dimensionless variables (four predictor variables and one response variable) according to the Buckingham Pi theorem [Gibbings, 2011]. However, four of the eight physical variables are usually assumed to be constant so one of these dimensionless variables will always be a constant or a linear combination of other variables. Assuming power-law forward equations between dimensionless variables, we assert that any choice of dimensionless variables can be rearranged to obtain the following dimensional equations:

$$q_b = \gamma_1 q_w^{\alpha_{11}} S^{\alpha_{12}} D_b^{\alpha_{13}} \quad (5)$$

$$C_s = \gamma_2 q_w^{\alpha_{21}} S^{\alpha_{22}} D_b^{\alpha_{23}} \quad (6)$$

$$D_s = \gamma_3 q_w^{\alpha_{31}} S^{\alpha_{32}} D_b^{\alpha_{33}} \quad (7)$$

where  $\gamma_1$ ,  $\gamma_2$ , and  $\gamma_3$  are fixed dimensional coefficients that can be expressed in terms of  $g$ ,  $\nu$ ,  $\rho_s$ , and  $\rho_w$ . This system of equations can then be solved to obtain equation (1), noting that  $\beta_i$  exponents are simply algebraic combinations of  $\alpha_{ij}$  exponents.

Based on these arguments, we offer the following interpretation of equation (1), leaving further discussion to Section 5.2. We assume changes in fluvial sediment transport conditions are driven by changes in  $q_w$ ,  $S$ , and  $D_b$ . By measuring one of these variables ( $q_w$ ) and two variables that directly respond to changes in these variables ( $C_s$  and  $D_s$ ), it is possible to constrain the state of the transport system and predict unknown variables including bedload flux. In this manner,  $C_s$  and  $D_s$  are viewed as proxies for  $S$  and  $D_b$ .

As an aside, equation (1) can also be derived by combining simplified relations presented in the canonical sediment transport literature [e.g. *Wong & Parker*, 2006; *Engelund & Hansen*, 1967; *Brownlie*, 1983; *Garcia & Parker*, 1991]; however, many of these relations have empirical origins and thus contain large, unquantifiable uncertainty. Rather than combining a series of existing empirical expressions, we fit  $\beta_i$  parameters and quantify predictive uncertainty directly; this approach minimizes predictive bias assuming that available data sufficiently capture the underlying physical processes.

The majority of this paper focuses on the development and application of a statistical methodology used to estimate empirical scaling parameters in equation (1) and predict bedload flux. We present an example application at our field site on the Colorado River in Grand Canyon National Park, where estimates of bedload flux obtained from repeat bathymetric surveys of dune migration paired with concurrent gage measurements form the observational basis for statistical analyses. Parameter estimation and prediction is conducted using Bayesian inference which facilitates consistent propagation of uncertainty from multiple sources of information and prediction of distributions for quantities of interest [Schmelter *et al.*, 2011; Schmelter & Stevens, 2012; Schmelter *et al.*, 2015]. This approach is particularly useful for propagating uncertainty arising from both measurement uncertainty and parameter estimation uncertainty in calculations of cumulative sediment load [Schmelter *et al.*, 2012].

In addition to the data from our site, we also consider data from six other rivers reported by Toffaleti [1968] in order to test generality and improve the predictive power of our model. These data cover a much wider range of discharge, slope, and bed grain size conditions than those that are found at the site on the Colorado River. In order to incorporate these data into the predictive model for bedload flux at our site, we consider three statistical models that are distinguished in principle by their assumptions regarding the universality of scaling exponents and in practice by their treatment of groups in the data. These approaches have advantages and disadvantages to each other relative to the specific modeling conditions and objectives, as well as the quantity and quality of data that are available at a site of interest.

### 3.2 Statistical methods

#### 3.2.1 Bayesian linear regression

The generalized linear model given by equation (1) has four unknown parameters that must be estimated from a large number of observations of model variables. This system is overdetermined and no single solution can fit all of the data simultaneously. As a result, it is necessary to employ regression analysis to handle uncertainty and error. Log-transformed variables enable linear regression, which assumes that the  $i^{th}$  observation of the response variable  $\log(q_b)_i$  can be expressed as a linear function of the predictor variables  $\log(Q)_i$ ,  $\log(C_s)_i$  and  $\log(D_s)_i$ , plus an error term  $\epsilon_i$

$$\log(q_b)_i = \log(A)_i + \beta_0 + \beta_1 \log(q_w)_i + \beta_2 \log(C_s)_i + \beta_3 \log(D_s)_i + \epsilon_i \quad (8)$$

Perhaps the most common variant of linear regression is Ordinary Least-Squares (OLS), which finds the combination of model parameters  $\beta_0$ ,  $\beta_1$ ,  $\beta_2$ , and  $\beta_3$  that minimizes the sum of the sum of the squared error terms. OLS regression leads to an unbiased predictor of the response variable assuming  $\epsilon_i$  is normally distributed and independent across all samples. However, for the purposes of the present research, this approach has several limitations. OLS regression cannot handle hierarchical organizations of data that potentially violate the assumed independence of  $\epsilon_i$ , such as when individual observations are grouped by river or site. Additionally, analytical quantification of predictive uncertainty in the OLS framework does not readily allow for propagation of errors through mass-balance calculations.

Bayesian inference provides a convenient framework for overcoming these issues. For a general discussion of Bayesian methods, see Gelman *et al.* [1995]; Christensen *et al.* [2011]. The standard Bayesian approach to linear regression starts with the same assumptions as OLS that are encapsulated by (8). However, we introduce an additional parameter  $\sigma$  that quantifies the standard deviation of the error term, i.e.:

$$\epsilon_i \sim \mathcal{N}(0, \sigma) \quad (9)$$

where the tilde means “distributed as” and  $\mathcal{N}(0, \sigma)$  is an independent normal distribution with zero mean and standard deviation  $\sigma$ . Consequently, we aim to draw inference on five parameters:  $\beta_0$ ,  $\beta_1$ ,  $\beta_2$ ,  $\beta_3$ , and  $\sigma$ .

At this point we note for clarity that the term “variables” refers to measurable physical quantities, while the term “parameters” refers to unknown quantities that appear in the data model and are the object of statistical inference. Henceforth, we use  $\theta$  to refer to the  $5 \times 1$  vector of model parameters, i.e.  $\theta = [\beta_0, \beta_1, \beta_2, \beta_3, \sigma]$ . Additionally, we use  $X$  to refer to the  $4 \times N$  matrix of  $N$  observations of model variables  $q_w$ ,  $C_s$ ,  $D_s$ , and  $q_b$ .

While OLS regression seeks estimates of model parameters that minimize the global sum of the squared residuals, Bayesian model fitting embraces uncertainty associated with the fact that small differences in model parameters may fit the data nearly as well as the optimal result. These small differences are quantified by the likelihood function, which

exists on the domain of model parameters assuming fixed observational data  $X$ , and is denoted by  $L(\theta|X)$ . Here, the vertical line denotes conditional dependence, i.e. the likelihood of  $\theta$  given  $X$ . The likelihood can be computed for any combination of parameters, where higher likelihoods represent more likely combinations of parameters. Introducing the prior probability distribution  $P(\theta)$ , we obtain an expression for the posterior probability distribution of model parameters conditional on observational data  $P(\theta|X)$  through Bayes theorem:

$$P(\theta|X) = \frac{L(\theta|X)P(\theta)}{\int L(\theta|X)P(\theta)d\theta} \quad (10)$$

Once the posterior probability distribution of model parameters is known, unobserved values of  $q_b$  can be estimated from measured values of predictor variables using Bayesian posterior predictive distributions, which efficiently propagate uncertainty through individual estimates of  $q_b$  as well as time-integrated mass-balance calculations.

### 3.2.2 Grouped, ungrouped, and hierarchical model variations

The basis for equation (1) suggests that it is sufficient to predict bedload flux in any sand bed river using a single universal set of scaling parameters. However, some degree of predictive uncertainty is inevitable owing to both measurement error and model bias arising from simplification of physical processes. While measurement error can be considered uncorrelated, systematic biases are caused by a failure of the data model to capture specific physical processes, and are thus likely to be correlated when conditions are similar. As a result, we anticipate persistent site-specific biases using a general model based on data from many rivers. For example, details of channel geometry not explained by width and slope may cause bedload flux to be more or less sensitive to changes in water discharge at one site compared with the central tendency of all sand bed rivers. In this case, better predictive accuracy would be achieved at that site by adjusting the value of  $\beta_1$  to reflect this difference. In general, we anticipate better predictive performance if model parameters are constrained on a site-specific basis.

This theoretical consideration is at odds with practical limitations: regression analysis requires numerous independent estimates of bedload flux that are expensive and difficult to obtain. Thus, it would be advantageous if existing data from many rivers could be used to help inform bedload prediction at a new site. Optimal model parameters may differ slightly from site to site; however, sand-bed rivers are all governed by the same general physical processes such that it is reasonable to expect that scaling parameters should be similar between rivers. In order to balance theoretical and practical concerns, we consider three distinct generative data models, each of which reflects a different trade-off between observational data requirements and assumptions regarding the generality of scaling parameters.

The first model (the grouped model, Appendix B.1) assumes a single universal set of model parameters  $\theta = [\beta_0, \beta_1, \beta_2, \beta_3, \sigma]$ . The standard deviation of the error term  $\sigma$  is the same for all data. All observations are therefore treated as independent observations from the same exchangeable group of observations. The advantage of this model is that it can be applied at a new site without collecting any additional data. However, it ignores the possibility of correlated errors by river or site, and is therefore subject to unquantifiable systematic biases when applied at a specific site without local data.

The second model (the ungrouped model, Appendix B.2) assigns different independent scaling parameters  $\theta_j = [\beta_{j0}, \beta_{j1}, \beta_{j2}, \beta_{j3}, \sigma_j]$ , for  $j = 1, \dots, m$  and  $m = 8$  is the number of data groups (i.e. independent sites). This is equivalent to performing grouped regression independently on a site-specific basis: each site is treated as an independent statistical entity comprising its own exchangeable group of observations. This model is perhaps the most theoretically conservative in that it assumes nothing with regard to physical similarity between sites. However, it is also the least practical in that it requires ex-

303 tensive uncorrelated observations of bedload flux from each monitoring site in order to  
 304 ensure reliable results, and cannot be applied at a site where bedload has never been mea-  
 305 sured directly.

306 The third model (the hierarchical model, Appendix B.3) assigns different regression  
 307 coefficients to each site, but assumes some degree of physical similarity between sites.  
 308 Observations are treated as exchangeable on a site-specific basis, and each site comes from  
 309 an exchangeable group of sites, that is, all sand bed rivers. We aim to draw inference, not  
 310 only on the behavior of individual sites, but also on the distribution of behaviors that can  
 311 be observed at different sites. Site-specific coefficients are thus determined partly by data  
 312 collected at that site, but are also informed by the behavior of other rivers which can re-  
 313 duce issues related to low sample size at one site if sufficient data exists at other sites. Hi-  
 314 erarchical organization is implemented through priors for the regression coefficients which  
 315 are assumed to be normally distributed with a mean and variance that reflects the cen-  
 316 tral tendency and variability of sand-bed rivers. This model lies somewhere between the  
 317 grouped and ungrouped models in terms of both theoretical assumptions and data require-  
 318 ments. Some data are useful in order to constrain bedload flux at a new site, but limited  
 319 observations are utilized to greater effect than in the ungrouped model.

### 320 3.2.3 *Priors*

321 Diffuse (i.e. wide, minimally informative) priors are commonly used to minimize  
 322 influence on model results, and are employed here for all three model variations. Diffuse  
 323 priors are effectively constant over the relevant parameter domain, which means that the  
 324 posterior distribution is essentially reflects a renormalization of the likelihood function,  
 325 preserving the relative log-likelihoods while ensuring the posterior integrates to 1. Due  
 326 to the relatively large sample size, our results are not sensitive to the specific choice of  
 327 diffuse prior.

328 Grouped and ungrouped regression models were fit using an approximation for Jef-  
 329 frey's prior, which is an attractive choice due its unique theoretical properties [Gelman *et*  
 330 *al.*, 1995; Christensen *et al.*, 2011]]. Jeffrey's prior is a uniform distribution on the domain  
 331 ( $\beta_0, \beta_1, \beta_2, \beta_3, \log(\sigma)$ ), which is an improper prior because it does not integrate to 1. Thus,  
 332 normal distributions centered on zero with large standard deviations are used to approx-  
 333 imate Jeffrey's prior because a normal distribution approaches a uniform distribution as  
 334 the standard deviation goes to infinity. Jeffrey's prior is also uniform  $\log(\sigma)$  meaning the  
 335 prior probability that the parameter is between 0.01 and 0.1 is the same as the probability  
 336 the parameter is between 0.1 and 1. The inverse gamma distribution approaches a uniform  
 337 distribution on  $\log(\sigma)$  as its parameters go to zero.

338 The hierarchical model structure is implemented through informative, dynamic pri-  
 339 ors, where the parameters for these priors are referred to as "hyperparameters". Inference  
 340 is drawn on parameters and hyperparameters simultaneously such that the hyperparameters  
 341 have their own prior and posterior probability distributions. Priors for hyperparameters, or  
 342 "hyperpriors" must be specified. Again, we utilized diffuse, minimally-informative hyper-  
 343 priors, the specific choice of which does not influence model results. For additional details  
 344 on priors and hyperpriors, see Appendices B.1, B.2, and B.3.

### 345 3.2.4 *Model fitting*

346 All three models were fit using Markov Chain Monte-Carlo (MCMC) sampling  
 347 methods. This technique is commonly used to sample the posterior distribution and con-  
 348 duct predictive simulation when analytical alternatives are cumbersome or impossible. For  
 349 additional details on MCMC sampling, see Appendix B.4 and example workflows [Ashley,  
 350 2019b].

### 351 3.2.5 Model selection

352 Quantitative comparison of predictive power is accomplished using the Deviance  
 353 Information Criterion (DIC, *Spiegelhalter et al.* [2002]; *Gelman et al.* [2014]), Appendix  
 354 B.6), a generalization of the Akaike Information Criterion that is suitable for comparing  
 355 the hierarchical and non-hierarchical models used here. DIC includes two terms: one  
 356 which quantifies in-sample predictive accuracy and one which corrects for model complex-  
 357 ity to approximate out-of-sample predictive accuracy under certain assumptions [*Gelman*  
 358 et al., 2014]. As a relative measure of predictive power, models with lower DIC are ex-  
 359 pected to have lower prediction error than models with higher DIC. However, DIC is not a  
 360 perfect measure of relative prediction error and is reported here (Table 2) to inform model  
 361 evaluation rather than as the sole discriminatory factor.

### 362 3.3 Field methods

363 Transport-related data were collected at one field site on the Colorado River in Grand  
 364 Canyon National Park during three field campaigns in the Spring and Summer of 2015,  
 365 as well as the Fall of 2016. The site (Figure 2) is located at river mile 225 in the vicin-  
 366 ity of USGS monitoring station 09404200 (Colorado River above Diamond Creek near  
 367 Peach Springs, AZ). Hereafter, we refer to this site informally as "Diamond Creek" or  
 368 the "Diamond Creek field site". Data include repeat bathymetric surveys of dune migra-  
 369 tion, ADCP surveys of flow velocity, suspended sediment and bed sediment samples, and  
 370 bed photographs for optical grain-size analysis [*Buscombe et al.*, 2010]. Concurrent gage  
 371 measurements of water discharge, suspended sand concentration, and grain size were also  
 372 collected following standard procedures during this time [*Rantz et al.*, 1982; *Topping &*  
 373 *Wright*, 2016].

374 Estimates of bedload flux were obtained using 320 high resolution, full-width bathy-  
 375 metric surveys of an approximately 400 meter reach adjacent to the Diamond Creek gag-  
 376 ing station. Surveys were collected using a 400 kHz Reson 7125 multibeam echo sounder  
 377 (MBES) which produces a swath comprised of 512 beams (each 1 x 0.5 degrees) across  
 378 a transverse subtended angle of 135 degrees. In order to map sonar returns onto a global  
 379 coordinate system, the location of the boat was tracked using a robotic Total Station refer-  
 380 enced to a fixed position on the bank, and a fiber-optic gyrocompass and inertial sensors  
 381 were used to calculate heading, roll, and pitch of the sonar head. Patch tests were con-  
 382 ducted before the surveys to determine the offset angles and timing latency between the  
 383 various system components. Bad soundings and sweep misalignments (due to, for exam-  
 384 ple, systematic side-lobe interference; and scattering of soundings by air bubbles, drifting  
 385 insects and other organic matter in the water) were identified by manual sweep editing  
 386 and systematically stepping through overlapping sweeps. Quality assurance assessments  
 387 were performed after the surveys by comparing selected soundings from all surveys over a  
 388 large, flat-topped rock located along the channel margin. The mean standard deviation of  
 389 soundings over this feature was 0.015 m and indicate a high level of survey precision. The  
 390 final, edited surveys used here are ungridded point clouds, where each point corresponds  
 391 to a valid sonar return from the river bed. More details about acquisition of MBES data  
 392 with this instrument and configuration are found in *Kaplinski et al.* [2009]; *Kaplinski et al.*  
 393 [2014], *Grams et al.* [2013, 2018], and *Buscombe et al.* [2014a,b]. Four example surveys  
 394 are plotted in Figure 3.

398 *Simons et al.* [1965] provide the method by which bathymetric data can be used to  
 399 generate bedload flux estimates. Their expression is given by:

$$400 q_b = (1 - p)V_c \frac{H_c}{2} + C, \quad (11)$$

401 where  $q_b$  [ $L^2 T^{-1}$ ] is the volumetric bedload flux per unit width,  $p$  [-] is the bed porosity  
 402 taken to be a constant 0.35,  $V_c$  [ $LT^{-1}$ ] is a characteristic bedform migration rate,  $H_c$  [ $L$ ]  
 403 is a characteristic bedform height, and  $C$  is a constant of integration assumed to be zero.

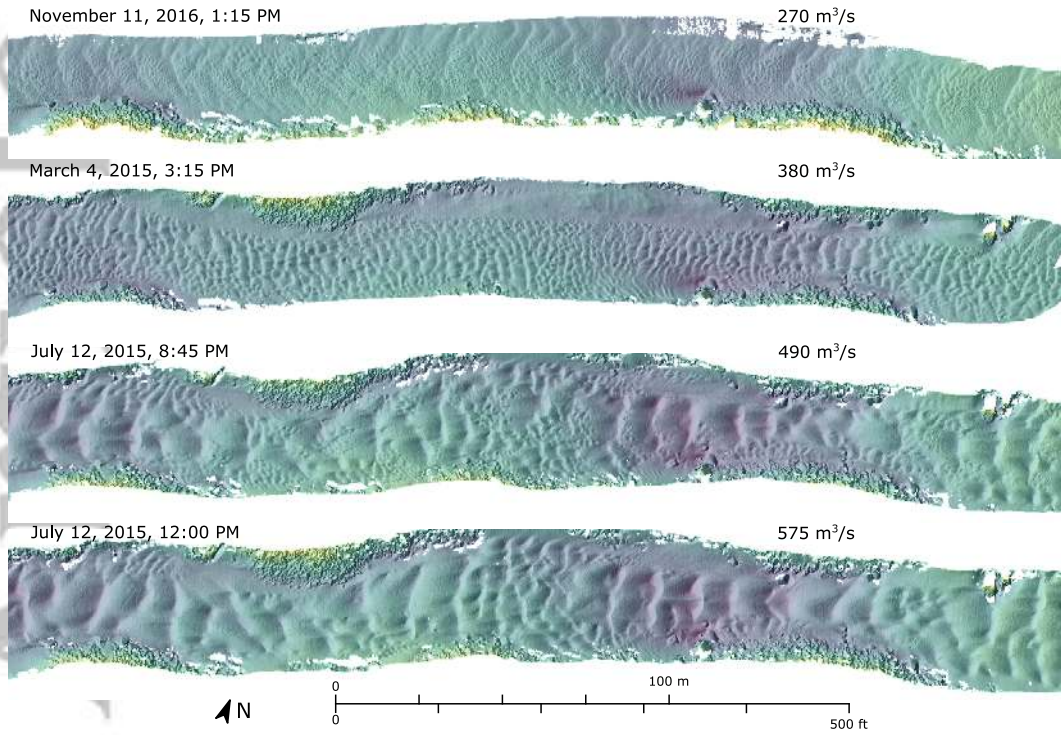


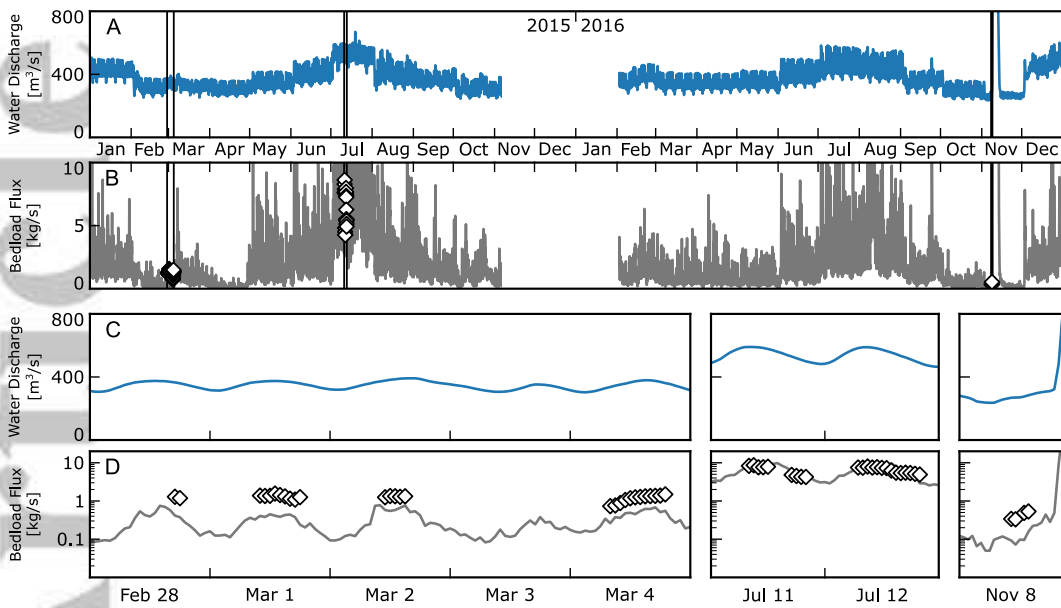
**Figure 3.** Example bathymetric surveys with shaded relief plotted at 10 cm resolution. Water discharge during the survey is indicated in the upper right corner of each survey. Flow is from right to left. Colors represent water depth, as in figure 2.

Measured bedform heights ranged from 0.15 to 0.70 m, and measured migration rates ranged from 0.21 to 1.76 m/hr. Both of these quantities varied predictably with water discharge.

Equation (11) is derived from a statement of mass conservation (the Exner equation, Paola & Voller [2005]) combined with a simplified model for dune evolution characterized by translationally invariant migration of triangular or sinusoidal forms. Although it represents substantial simplifications of physical process (for example, by ignoring bedform deformation and variability in bedform migration rate and geometry), flume and field studies find good agreement between (11) and other estimates of bedload flux across a wide range of conditions extending from the threshold of bedform development to suspension-dominated dunes [Simons *et al.*, 1965; Engel & Lau, 1980; *van den Berg*, 1987; Mohrig & Smith, 1996]. Consequently, we argue that this expression provides a reasonable estimate of bedload transport that is not captured by acoustic estimates of suspended sand load. Equation (11) was used to compute 55 hourly estimates of average bedload flux (Figure 4). Major elements of this procedure are discussed in Appendix A. Additional details can be found in the documentation of software developed for this purpose [Ashley, 2019a]

### 3.4 Additional data from other rivers

The large river dataset presented by Toffaleti [1968] (and derived quantities) is used to supplement limited data from our field site. This dataset comprises a total of 262 concurrent observations of bedload flux  $Q_b$ , water discharge  $Q_w$ , suspended sand concentration  $C_s$ , median suspended sand diameter  $D_s$ , and channel width  $W$  on the Atchafalaya River ( $n = 60$ ), the Mississippi River in Louisiana ( $n = 47$ ), the Mississippi River in Mis-



419 **Figure 4.** Time series plot of water discharge (A) and bedload flux (B) at the Diamond Creek sediment  
 420 monitoring station in 20015 and 2016. Grey line shows bedload flux estimated as a constant fraction (5%) of  
 421 suspended load, and black diamond show hourly average estimates of bedload flux from bedform migration.  
 422 Insets (C, D) highlight the periods where bedform flux estimates are available.

429 souri ( $n = 63$ ), the Red River ( $n = 28$ ), the Rio Grand River ( $n = 36$ ), the Middle Loup  
 430 River ( $n = 9$ ), and the Niobrara River ( $n = 19$ ). These sites are similar to the Diamond  
 431 Creek field site in that the predominant bed material is sand; however they are different in  
 432 that they are all alluvial rivers (whereas the Colorado River in Grand Canyon is a bedrock-  
 433 confined alluvial river with gravelly and sandy reaches). Our model is based on physical  
 434 theory describing one-dimensional transport, and assumes nothing about channel form.  
 435 Consequently, it can be applied in rivers that are not fully alluvial as long as the bed ma-  
 436 terial at the site of interest is sand.

437 Total suspended sand concentration  $C_s$  and median suspended sand grain size  $D_s$   
 438 were computed from reported grain-size specific suspended sediment concentrations. Bed-  
 439 load flux was computed according to the revised Meyer-Peter & Müller bedload equation  
 440 [Wong & Parker, 2006] with grain stresses estimated using the Einstein drag partition as  
 441 reformulated by Garcia [2008]. This procedure was also used to compute bedload flux at  
 442 our study site when flow velocity and bed sediment data are available to check approx-  
 443 imate correspondence with estimates of flux from dune migration. Note that here, and  
 444 throughout, “observations” is used as part of the statistical vernacular to refer to indepen-  
 445 dent samples of variables and implies nothing about how those samples were obtained.  
 446 This distinction is particularly important here because “observations” of bedload flux are  
 447 actually computed from depth, slope, grain size, and flow velocity using physically-based  
 448 model. Similarly, observations of bedload flux at Diamond Creek are computed using a  
 449 physically-based model from dune height and velocity.

### 451 3.5 Data treatment

452 The statistical methods employed here assume errors in observations are uncor-  
 453 related. However, the 55 hourly estimates of average bedload flux from the Diamond Creek  
 454 field site were collected over seven days during which temporal correlation is likely. Un-

450

**Table 1.** Summary of variable ranges measured at each site

	$Q_w$ [ $m^3/s$ ]		$W$ [m]		$\log_{10}(S)$		$D_b$ [mm]	
	min	max	min	max	min	max	min	max
Atchafalaya River	931	14186	314	503	-5.0	-4.3	0.10	0.41
Mississippi @ Tarbert Landing	4248	28827	896	1414	-4.7	-4.4	0.20	0.38
Mississippi @ St. Louis	1512	8778	457	518	-5.0	-3.2	0.20	0.86
Red River	190	2826	130	183	-4.2	-3.1	0.11	0.28
Rio Grande River	35	286	41	198	-3.1	-3.0	0.25	0.45
Middle Loup River	9	14	22	46	-2.9	-2.7	0.34	0.48
Niobrara River	6	21	19	41	-2.9	-2.7	0.30	0.40
Colorado @ Diamond Creek	267	590	59	64	-4.0	-3.7	0.30	0.50
	$q_w$ [ $m^2/s$ ]		$C_s$ [ppm]		$D_s$ [mm]		$Q_b$ [kg/s]	
	min	max	min	max	min	max	min	max
Atchafalaya River	2.9	28.6	4	372	0.08	0.16	0.20	12.5
Mississippi @ Tarbert Landing	4.7	24.2	5	199	0.10	0.18	0.43	6.7
Mississippi @ St. Louis	3.3	17.2	13	307	0.10	0.25	0.63	11.6
Red River	1.2	20.1	8	495	0.09	0.12	0.10	3.3
Rio Grande River	0.3	3.4	373	3177	0.12	0.22	1.5	41.1
Middle Loup River	0.2	0.6	183	1032	0.13	0.18	1.8	7.8
Niobrara River	0.2	0.9	189	1088	0.08	0.18	1.0	11.0
Colorado @ Diamond Creek	4.5	9.1	2	135	0.12	0.22	0.33	8.6

455

qualified extrapolation of trends in this dataset to the full gage record spanning nearly ten years may therefore produce unrealistic results. In order to mitigate this effect, we use only the first and last measurement from each day ( $n = 14$ ) in order to estimate model parameters.

456

457

458

The full data set used for statistical analysis comprises a total of 276 observations from eight sites. Data were log-transformed to obtain the linear regression variables  $q_w^*$ ,  $C_s^*$ ,  $D_s^*$ , and  $q_b^*$  using fixed reference values of each variable (Figure 5). We chose to use a single reference values for each variable (as opposed to individual reference values for each site) computed as the geometric mean of all 276 pooled observations of each variable, which results in centered (zero mean) log-transformed variables. Other choices may provide additional insight (if for example, different physically important reference values are used on a site-specific basis like mean annual discharge or bankfull discharge); however, such analyses are beyond the scope of this paper. Reference values of model variables are given by:  $q_{b0} = 0.039 \text{ kg/s/m}$ ,  $q_{w0} = 4.35 \text{ m}^2/\text{s}$ ,  $C_{s0} = 1.07 \times 10^{-4}$ , and  $D_{s0} = 0.13 \text{ mm}$ . Channel widths were computed using an empirical power-law function of water discharge at the Diamond Creek field site. Reported widths were used at other sites.

459

460

461

462

463

464

465

466

467

468

469

470

Here, we emphasize that the full dataset contains observations of bedload flux that were obtained using two very different methods. Bedload was estimated from grain stresses computed using the Einstein drag partition and the Wong & Parker bedload equation for the large river dataset reported by Toffaleti [1968], while bedload flux at Diamond Creek was computed using observations of bedform migration. For the purposes of statistical analysis, we assume both methods produce unbiased estimates of bedload flux with comparable uncertainty. Consequently, both methods are treated identically in the context of inference and prediction.

471

472

473

474

475

476

477

478

Accepted Article

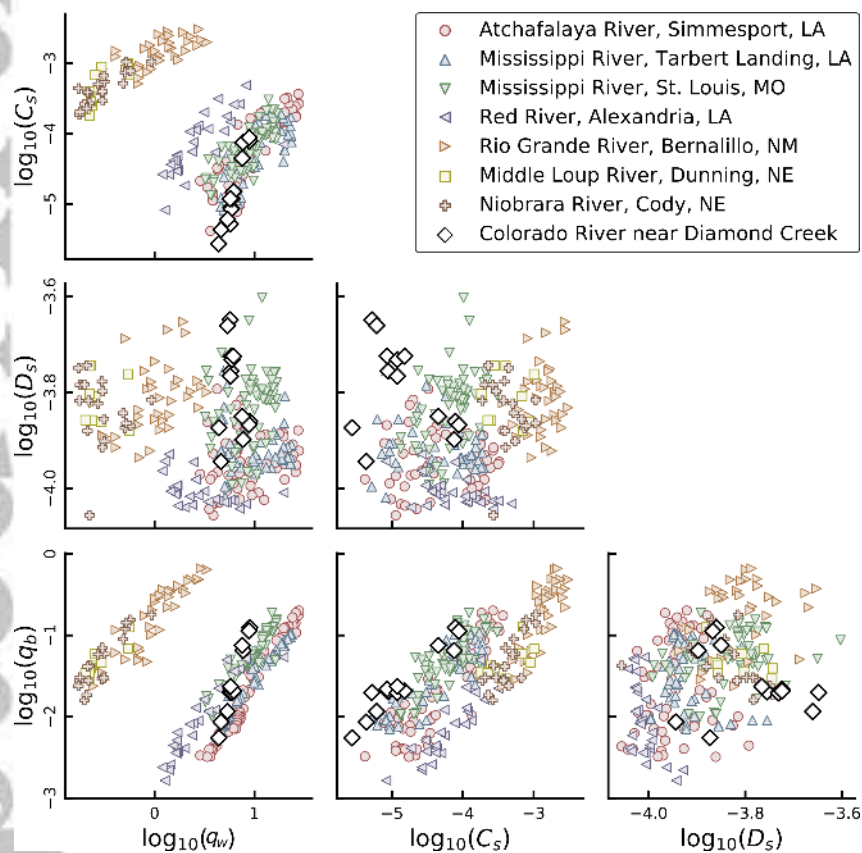


**Figure 5.** Expanded visualization of regression data. Pale colored markers indicate values of model variables computed from data reported by Toffaletti [1968]. Note that predictor variables ( $q_w$ ,  $C_S$  and  $D_S$ ) cover a wide range of conditions and are only weakly correlated when viewed collectively. Site-specific correlations are evident, especially between  $C_S$  and  $q_w$

483 **4 Results**

484 **4.1 Bedload fluxes at Diamond Creek**

485 Bedload flux computed from bedform migration is similar to bedload flux estimated  
 486 as a constant 5% of suspended sand load during the July 2015 survey period, correspond-  
 487 ing to the highest water discharges observed ( $450 \text{ m}^3/\text{s}$  to  $600 \text{ m}^3/\text{s}$ ). Bedload fractions  
 488 are significantly higher during the March 2015 and November 2016 survey periods, cor-  
 489 responding to lower water discharges ( $275 \text{ m}^3/\text{s}$  to  $400 \text{ m}^3/\text{s}$ ). Bedload flux ranged from  
 490  $0.33 \text{ kg/s}$  to  $8.6 \text{ kg/s}$  during the various data collection intervals (Figure 4). The bedload  
 491 fraction is negatively correlated with suspended sand flux, ranging from as little as 3% to  
 492 as much as 26% of suspended sand flux.

493 **4.2 Inference on model parameters**

494 Kernel density estimates of the marginal posterior distributions of model parameters  
 495 are plotted in Figure (6). The statistical effect of each predictor variable is quantified  
 496 by the value of the  $\beta$  exponent corresponding to that variable. Peaked distributions indi-  
 497 cate low parameter estimation uncertainty, and wide distributions indicate high uncertainty.  
 498 Median parameter estimates are reported in Table 2.

499 Computed DIC values indicate that the hierarchical model has the lowest expected  
 500 prediction error averaged across all sites. In order to evaluate the effect of each parameter  
 501 on predictive power, we computed DIC using permutations of each model involving only  
 502 two predictor variables. The predictive power using the grouped model is significantly re-  
 503duced using any of the two-variable permutations. However, we find that the predictive  
 504 power of the ungrouped model is improved by ignoring  $D_s^*$  (DIC = 298 compared to 382).  
 505 This indicates that considering  $D_s^*$  does not improve model fit enough to justify the added  
 506 complexity. Excluding  $D_s^*$  has essentially no effect on the predictive power of the hierar-  
 507 chical model (DIC = 112 compared to 123).

509 **4.3 Prediction**

510 Predictive distributions of total mass bedload flux (Appendix B.5) were computed  
 511 using all three models using hourly-average measurements of  $Q$ ,  $C_s$ , and  $D_s$  recorded at  
 512 the Diamond Creek gage from January 1, 2008 to December 31, 2016. This was accom-  
 513 plished by computing full posterior predictive distributions for each gage measurement of  
 514 model variables. Median predictions are compared against observational data in Figure  
 515 (7). The full simulated time series of bedload flux, the ratio of bedload to suspended load,  
 516 and predictor variables are plotted in Figure (8).

529 **5 Discussion**

530 **5.1 Comparison of model variations**

531 We have presented three variations on our generalized bedload modeling framework  
 532 that differ in their assumptions, implementation, and interpretation. Here, we compare  
 533 model variations in the context of the statistical inference and predictions reported in Sec-  
 534 tion 4.

535 The grouped model most closely encapsulates the physical reasoning presented in  
 536 Section 3.1, which argues that quasi-universal relationships between transport parameters  
 537 emerge through the processes governing their interaction and equilibration. These rela-  
 538 tionships comprise three primary modes of variability driven by water discharge, channel  
 539 geometry, and bed composition. Three predictor variables improve predictive power com-  
 540 pared with any two-parameter model permutation, indicating that that all three modes of  
 541 variability are represented in the data.

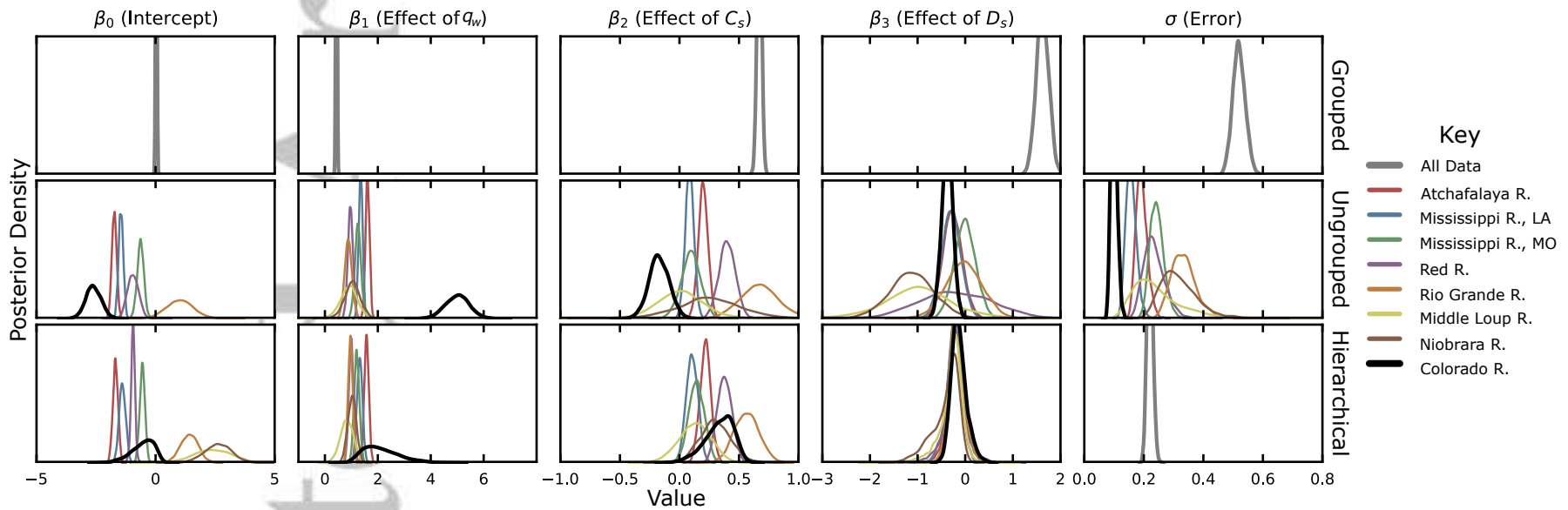
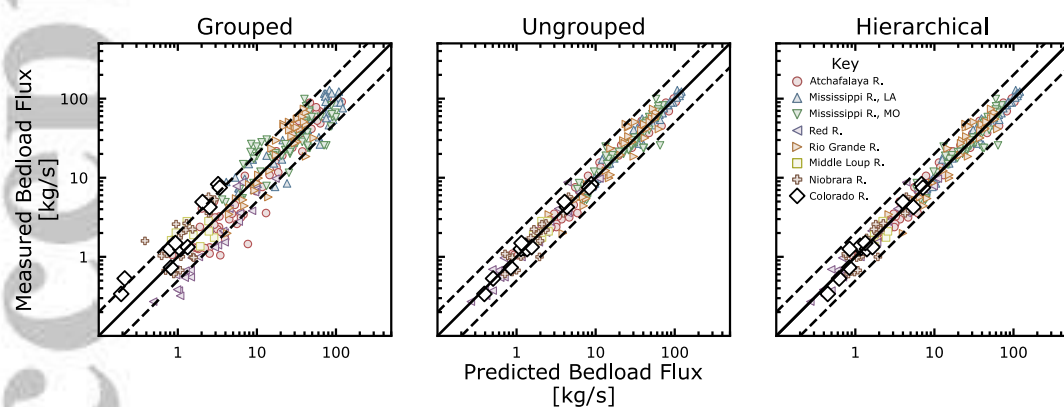


**Figure 6.** Marginal posterior distributions for model parameters. Distribution widths indicate parameter estimation uncertainty. The grouped model uses a single set of parameters to describe all data, while ungrouped and hierarchical model variations involve fitting separate regression parameters to each site. Note that site-specific posterior distributions are more clustered for the hierarchical model than for the ungrouped model owing to the dynamic, informative priors for the regression coefficients.

508

**Table 2.** Median posterior parameter estimates

Location	$\beta_0$	$\beta_1$	$\beta_2$	$\beta_3$	$\sigma$
Grouped Model (DIC = 552)					
All	0.08	0.048	0.68	1.65	0.52
Ungrouped Model (DIC = 382)					
Atchafalaya River	-1.68	1.65	0.21	-0.24	0.20
Mississippi @ Tarbert Landing	-1.41	1.39	0.09	-0.27	0.16
Mississippi @ St. Louis	-0.58	1.29	0.11	0.02	0.25
Red River	-0.90	1.01	0.41	-0.18	0.24
Rio Grande River	1.07	0.92	0.68	0.01	0.34
Middle Loup River	2.95	0.95	0.02	-0.96	0.26
Niobrara River	2.84	1.08	0.27	-1.10	0.32
Colorado @ Diamond Creek	-2.56	5.04	-0.16	-0.35	0.10
Hierarchical Model (DIC = 123)					
Atchafalaya River	-1.63	1.61	0.22	-0.19	0.22
Mississippi @ Tarbert Landing	-1.35	1.36	0.11	-0.20	0.22
Mississippi @ St. Louis	-0.51	1.24	0.15	-0.16	0.22
Red River	-0.90	1.04	0.39	-0.19	0.22
Rio Grande River	1.47	1.01	0.57	-0.16	0.22
Middle Loup River	2.45	0.87	0.14	-0.22	0.22
Niobrara River	2.68	1.07	0.31	-0.30	0.22
Colorado @ Diamond Creek	-0.43	2.07	0.36	-0.12	0.22
$\mu_k$	0.19	1.30	0.28	-0.21	
$\sigma_k$	1.83	0.44	0.18	0.11	



517

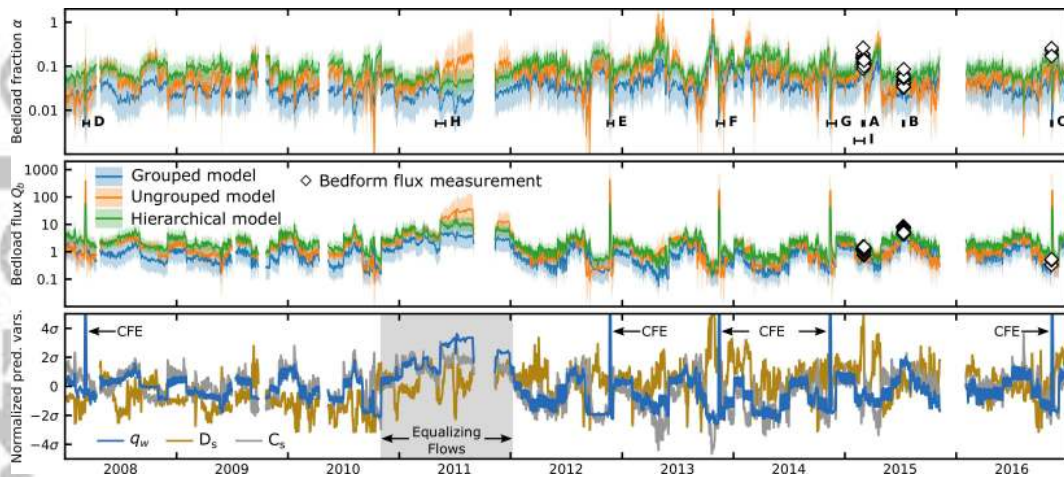
518

519

520

521

**Figure 7.** Plot comparing predicted and observed bedload flux. Predictions reflect median parameter estimates. Dashed lines indicate a factor of two deviation between predicted and observed bedload flux. Note that the ungrouped and hierarchical models provide improved fit compared with the grouped model. The hierarchical model leads to more precise estimates of model parameters while providing similar fit to the data when compared with the ungrouped model.



522 **Figure 8.** Simulated hourly-averaged bedload fraction (upper panel), bedload flux (middle panel) and  
 523 predictors (lower panel) over the full gage record. Dark lines represent the median of  
 524 the predictive distribution for bedload flux. Shaded regions represent 95% prediction intervals.  
 525 Bracketed segments denoted A through I are plotted in Figures (9), (10), and (11). Plotted predictor variables are log-  
 526 transformed and then normalized by subtracting the mean and dividing by the standard deviation. Controlled  
 527 flood experiments (CFE's) and elevated "equalizing flows" used to balance reservoir levels are also indicated  
 528 in the bottom panel.

542 In principle, the grouped model can be applied at any site to predict bedload flux,  
 543 including new sites that lack direct observational data. However, while individual pre-  
 544 dictions are unbiased relative to the full dataset, systematic biases exist among groups of  
 545 measurements that come from a single site; for example, the grouped model under-predicts  
 546 bedload flux at the Diamond Creek field site (Figure 7). Systematic biases are prob-  
 547 lematically when computing sediment budgets because they accumulate over time to cause com-  
 548 pounded errors.

549 By considering each site separately, the ungrouped and hierarchical models reduce  
 550 site-specific systematic biases. They also reflect a restricted scope of physical process:  
 551 while the grouped model represents quasi-universal physical relationships across many  
 552 sites, the ungrouped and hierarchical models capture site-specific associations between  
 553 variables. As a result, we find that two-parameter permutations of the grouped and hier-  
 554 archical models (ignoring  $D_s$ ) provide equal or better predictive power than the general-  
 555 ized three-parameter approach. This observation can be explained by the fact that slope  
 556 is effectively fixed at each site over human timescales in comparison to the differences  
 557 observed between rivers, reducing the number of principle modes of variability to two.  
 558 These modes are driven by fluctuations in flow strength and sediment supply, where sedi-  
 559 ment supply influences fluxes through both "grain size and reach-geometric effects" (*sensu*  
 560 Topping *et al.* [2000a,b]). This finding is potentially valuable for sediment monitoring pur-  
 561 poses because measurements of  $C_s$  are significantly easier to obtain than measurements of  
 562  $D_s$ .  $C_s$  varies by many orders of magnitude and can be measured accurately using single-  
 563 frequency instruments in a wide range of conditions, while  $D_s$  requires well sorted sus-  
 564 pended material, two-frequency instrumentation, and is only accurate for a small range of  
 565 grain sizes [Topping & Wright, 2016].

566 The hierarchical model differs from the ungrouped model in that the site-specific  
 567 associations between variables are assumed to be similar between sites. Through this as-  
 568 sumption, sites with many observations inform prediction at sites with relatively few ob-

569 servations. This effect is most clear at our field site, where few observations ( $n = 14$ ) lead  
 570 to spurious point estimates of regression parameters (Table 2) and large uncertainty (Figure 6) using the ungrouped model. The hierarchical model produces a slightly poorer fit to  
 571 the data but yields much more precise and consistent estimates of regression parameters.  
 572

573 In summary, each model has a specific set of assumptions, data requirements, and  
 574 limitations that must be evaluated in order to be applied to a specific problem. The grouped  
 575 model reflects quasi-universal physical relationships between variables and can be applied  
 576 at any site without training data but introduces systematic bias to cumulative bedload esti-  
 577 mates. The ungrouped model minimizes site-specific, systematic biases and assumes nothing  
 578 about similarity between sites but requires extensive observational data to be applied  
 579 at a given site. The hierarchical model reduces the number of observations needed at a  
 580 site relative to the ungrouped model under the assumption that sites are similar. Grouped  
 581 and hierarchical models can potentially be applied using only measurements of  $Q_w$  and  
 582  $C_s$ .

583 Presently, we aim to compute sediment budgets over the full gage record at the Di-  
 584 amond Creek sediment monitoring station. We argue that the hierarchical model is the  
 585 best choice for this purpose because it reduces systematic bias but provides efficient use of  
 586 limited data. Time series predictions made using the hierarchical model are plotted over  
 587 select intervals in Figures (9), (10), and (11).

## 588 5.2 Comparison with existing methods for estimating bedload flux

589 Prior to this research, the two primary methods for estimating bedload flux from  
 590 gage data in practical applications are (1) rating curves with discharge [e.g., Leopold &  
 591 Maddock, 1953; Emmett & Wolman, 2001] and (2) constant bedload coefficients based on  
 592 continuous measurements of  $C_s$  [e.g., Rubin *et al.*, 2001; Grams *et al.*, 2013]. To highlight  
 593 the advantages of the model presented here, we compare simulated bedload time series  
 594 with rating curve and bedload coefficient predictions. Several short example intervals were  
 595 selected for this purpose and are plotted in Figures (10) and (11).

596 Both approaches are special cases of our general model (equation 1), wherein cer-  
 597 tain parameters are fixed. For example, rating curves express bedload flux as a power-law  
 598 function of water discharge, i.e.:

$$Q_b = k Q_w^m \quad (12)$$

599 which is similar to equation (1) with null coefficients on suspended sand concentration  $C_s$   
 600 and diameter  $D_s$ :

$$q_b = A e^{\beta_0} q_w^{\beta_1} C_s^0 D_s^0 W^{1-\beta_1}. \quad (13)$$

601 Assuming width scales with discharge ( $W = a Q_w^b$ ), this reduces to

$$Q_b = (A e^{\beta_0} a^{1-\beta_1}) Q_w^{\beta_1 + b(1-\beta_1)}. \quad (14)$$

602 Here,  $k = A e^{\beta_0} a^{1-\beta_1}$  and  $m = \beta_1 + b(1-\beta_1)$  are assumed to be constant. For the purposes  
 603 of comparing rating curve and hierarchical predictions, rating curve parameters ( $k$  and  $m$ )  
 604 were found using ordinary least-squares regression applied to concurrent observations of  
 605 water discharge and bedload flux obtained at the gaging station and from repeat surveys  
 606 of dune migration, respectively. By specifying  $\beta_2 = 0$  and  $\beta_3 = 0$ , rating curves assume  
 607 a unique relationship between bed composition, channel geometry, and discharge, which  
 608 is problematic because sediment supply limitation is known to modify the transport effi-  
 609 ciency of a given discharge through reach-geometric and grain size effects [Topping *et al.*,  
 610 2000a,b]. Sediment supply variability can thus cause systematic deviations from rating-  
 611 curve predictions; pulses of fine bed material result in an enriched state characterized by  
 612 increased bedload flux. Subsequent preferential evacuation of fine material produces a de-  
 613 pleted state during which bedload flux is suppressed relative to a hypothetical discharge  
 614 rating curve prediction (Figure 12). Our modeling approach provides the potential to cap-  
 615 ture the effects of sediment supply limitation parameterized by  $C_s$  and  $D_s$ . As a result, we

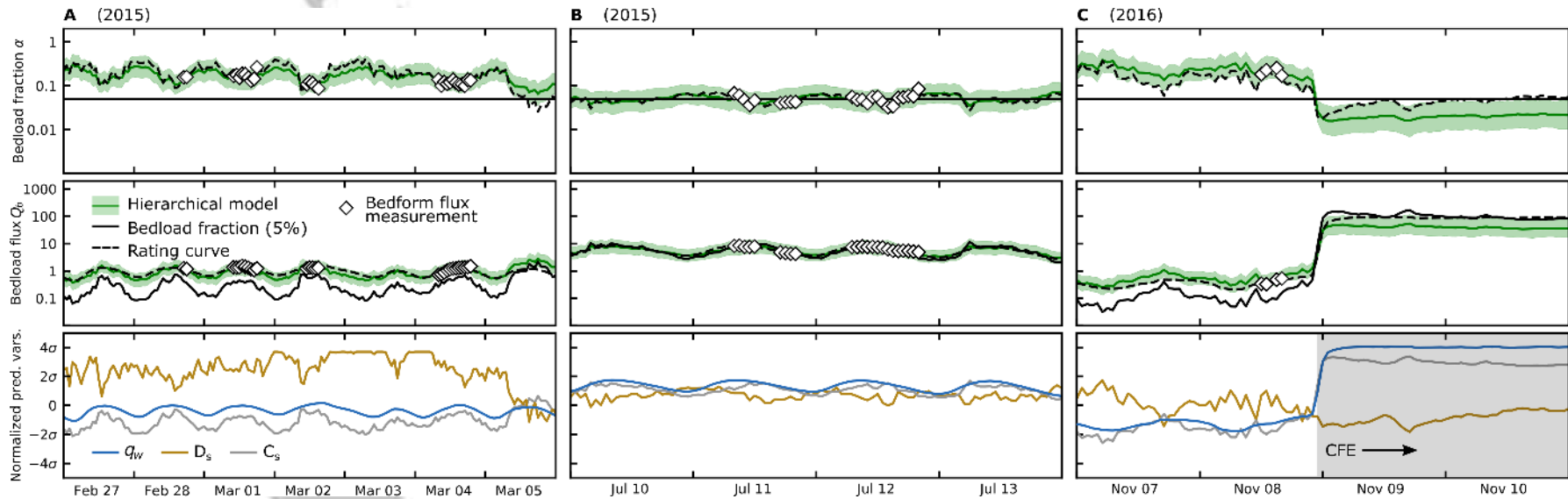


**Figure 9.** Simulated bedload fraction (upper panel), bedload flux (middle panel) and predictor variables (lower panel) at fifteen-minute resolution during the periods where observations of bedload flux from bedform migration are available. Plotted predictor variables are log-transformed and then normalized by subtracting the mean and dividing by the standard deviation.

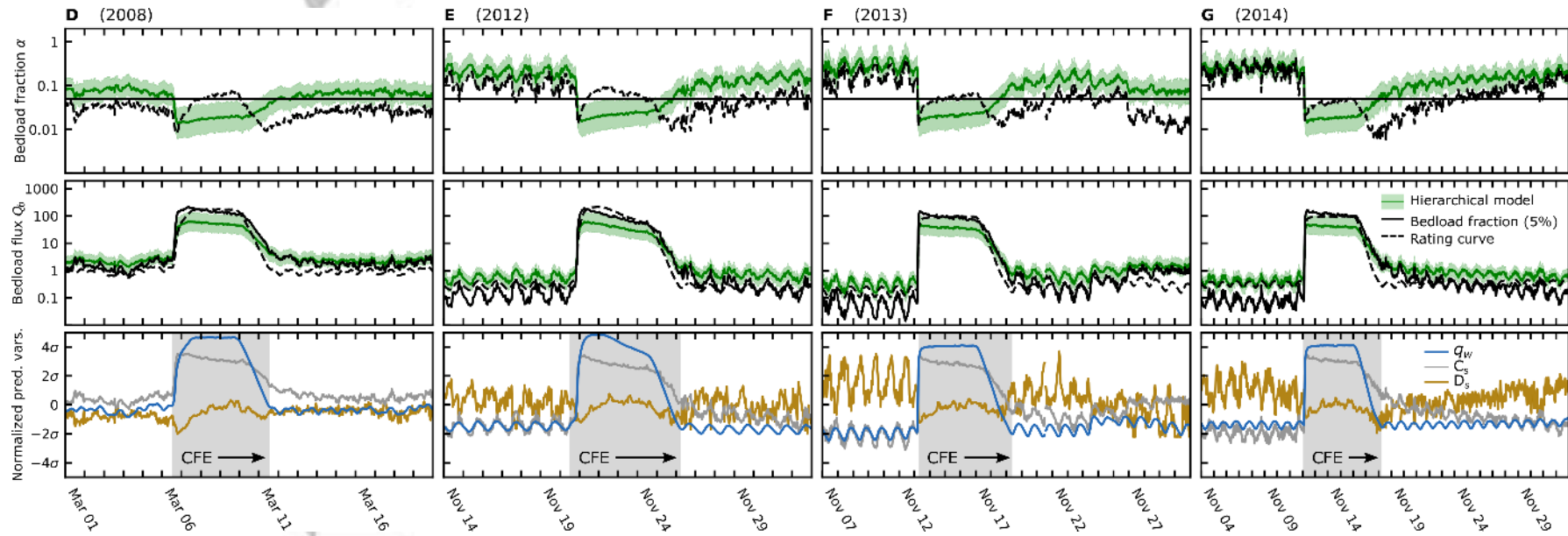


**Figure 10.** Simulated bedload fraction (upper panel), bedload flux (middle panel) and transformed predictor variables (lower panel) for the periods surrounding controlled flood experiments (CFEs).

interpret the difference between hierarchical model predictions and rating curve predictions as an indicator of the relative supply-limitation state of the Diamond Creek sediment monitoring reach: a positive difference is indicative of relative enrichment of fine sand whereas a negative difference is indicative of relative depletion.

Such enrichments or depletions are particularly pronounced during and after controlled flood experiments (Figure 10). For example, the period following each controlled flood typically records finer suspended sand grain sizes and elevated suspended sand concentrations relative to antecedent conditions, indicating fine-sediment enrichment [Rubin & Topping, 2001]. This is perhaps caused by delivery of fine material accessed above the typical high water line and/or the reworking of existing alluvial deposits in a manner that increases transport efficiency. Hierarchical model predictions are correspondingly elevated relative to rating curve predictions following each controlled flood.

Bedload coefficients are sometimes used to account for the contribution of bedload to total load in scenarios where measurements of suspended flux are available and bedload is thought to be small [e.g., Grams et al., 2013]. In order to estimate total load, researchers sometimes apply a universal correction factor  $1 + \alpha$  to measurements of suspended sand flux  $Q_s$ , which implies

$$q_b = \alpha q_s. \quad (15)$$

Noting that  $q_s = q_w C_s$ , equation (15) is a special case of the our general bedload model (1) wherein  $\beta_1 = 1$ ,  $\beta_2 = 1$ , and  $\beta_3 = 0$ , i.e.:

$$q_b = A e^{\beta_0} q_w^1 C_s^1 D_s^0. \quad (16)$$

Here,  $\alpha = A e^{\beta_0}$  is the constant bedload coefficient. In some sense, this expression represents a crude attempt to account for supply limitation effects by assuming bedload and suspended load are equally sensitive to changes in their mutual causal predictors (water discharge, channel geometry, and bed composition). However, suspension conditions (parameterized by the Rouse number,  $Z_R = w_s / \kappa u_*$ , where  $w_s$  is the particle settling velocity,  $u_*$  is the basal shear velocity, and  $\kappa$  is von Karman's constant) vary with flow strength and sediment supply, and are the most important predictor of  $\alpha$  (van Rijn [1984], Equation 45). Insofar as the Rouse number may vary over time at a site, it is unreasonable to expect that the bedload fraction should remain constant. Instead, increasing  $Z_R$  should generally cause an increase in  $\alpha$ . This may occur due to changes in  $u_*$  (as a function of water discharge, channel geometry, and bed roughness), or due to changes in  $w_s$ , which is a monotonically increasing function of  $D_b$ .

Comparison of hierarchical model and bedload coefficient predictions reveals several expected behaviors. In general, elevated suspended sand fluxes tend to correspond to increased suspension conditions (low Rouse numbers) and low bedload fractions (Figure 13). Bedload flux is a larger fraction of total load when discharge is low, corresponding to higher Rouse numbers due to decreases in  $u_*$ . Sediment supply depletion also increases the bedload fraction when discharge is held constant, corresponding to higher Rouse numbers due to increases in  $w_s$ . Discharge effects are most pronounced before, during, and after controlled flood experiments (Figure 10), which exemplify both the high and low bedload fraction extremes. Supply limitation effects are evident during long periods of nearly constant discharge which tend to be associated with gradual sediment-supply depletion (Figure 11). Gradual depletion causes a concurrent increase in the bedload fraction which is also apparent after the 2014 controlled flood experiment (Figure 10).

### 5.3 Management implications

Sediment budgets are used to estimate changes in stored sediment mass over a wide range of timescales. Short term effects of interest include perturbations related to dam-regulated water discharge or tributary sand delivery. Serendipitously (in the context of 5% bedload coefficients used by Rubin et al. [2001]; Topping et al. [2010]; Grams et al.

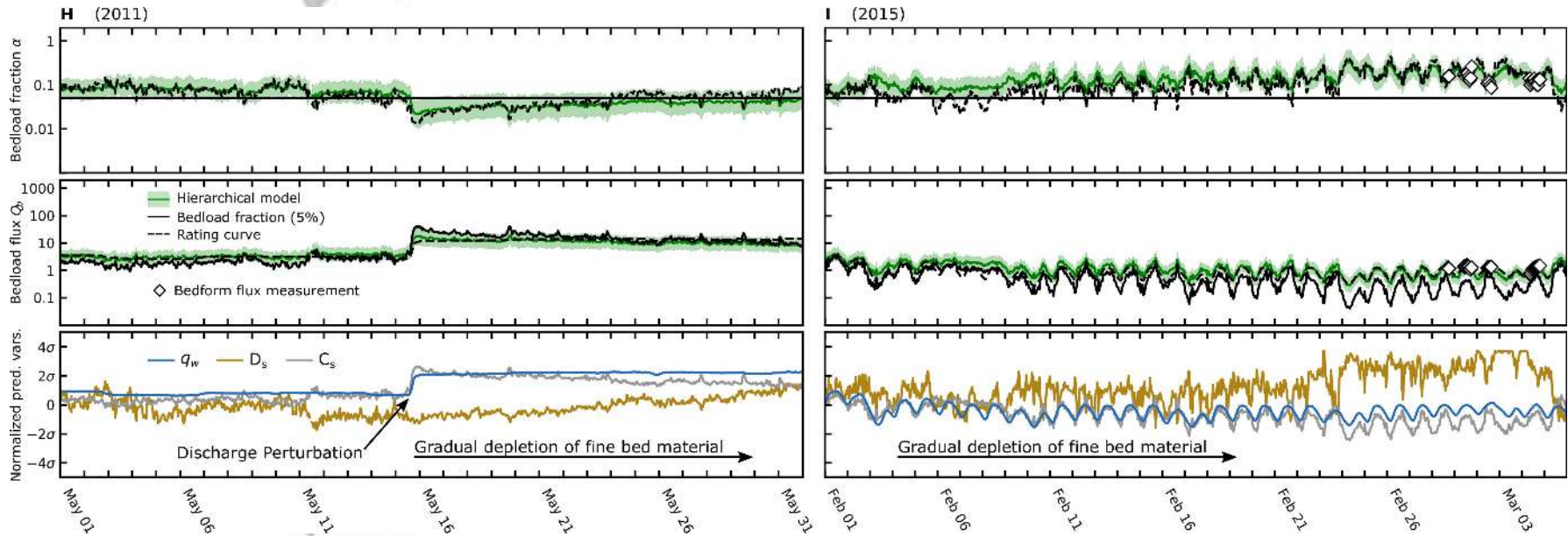
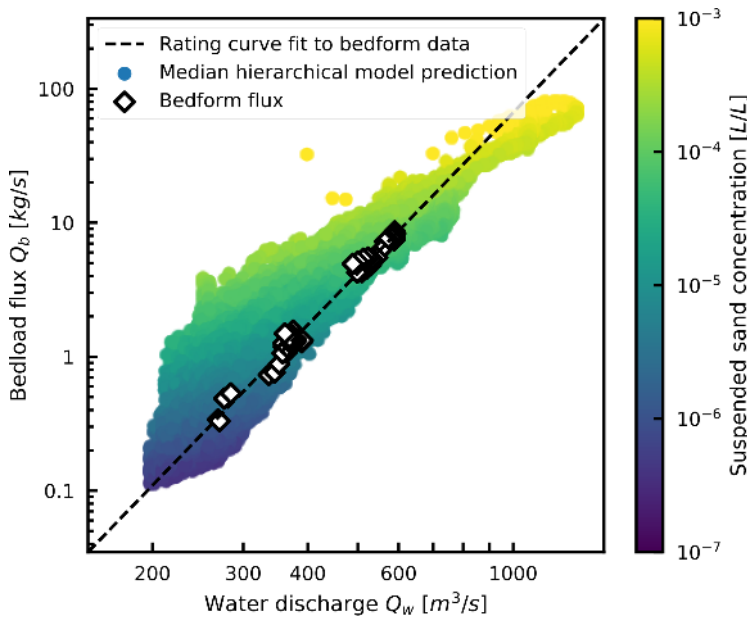
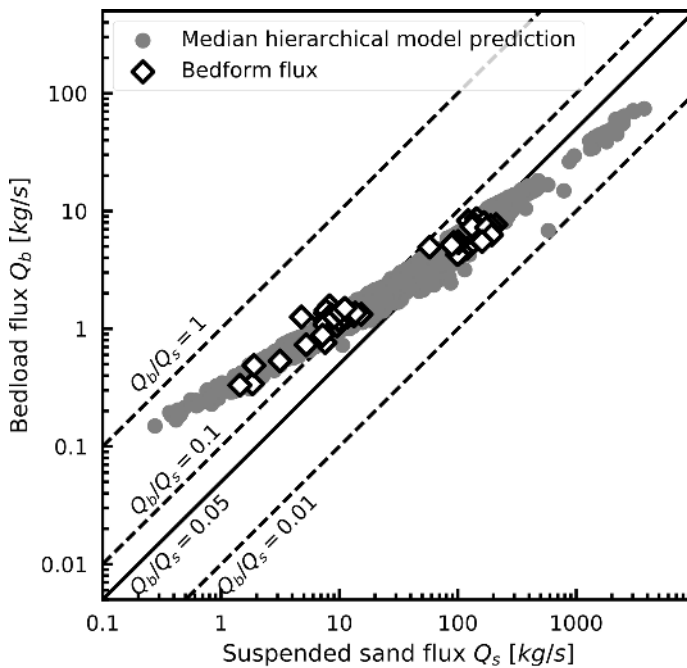


**Figure 11.** Simulated bedload fraction (upper panel), bedload flux (middle panel) and transformed predictor variables (lower panel) for two periods that record gradual coarsening of bed material under nearly constant (H) and periodically-fluctuating (I) flow conditions.



628 **Figure 12.** Plot illustrating the advantages of the proposed model over a traditional rating curve approach.  
 629 Note that predicted bedload flux may vary by over an order of magnitude with respect to a fixed water dis-  
 630 charge, an effect that is typically attributed to supply-limitation effects. Suspended sand concentration is  
 631 connected to the supply-limitation state of a reach; here, elevated suspended sand concentrations indicative of  
 632 fine-sediment enrichment and amplified bedload flux.



652 **Figure 13.** Plot illustrating the advantages of the proposed model over a constant bedload fraction ap-  
 653 proach. Diagonal lines show contours of constant bedload fraction. The predicted (and to a lesser extent,  
 654 measured) trend seen here is consistent with the notion that high suspended sand fluxes correspond to elevated  
 655 suspension conditions and lower bedload fractions.

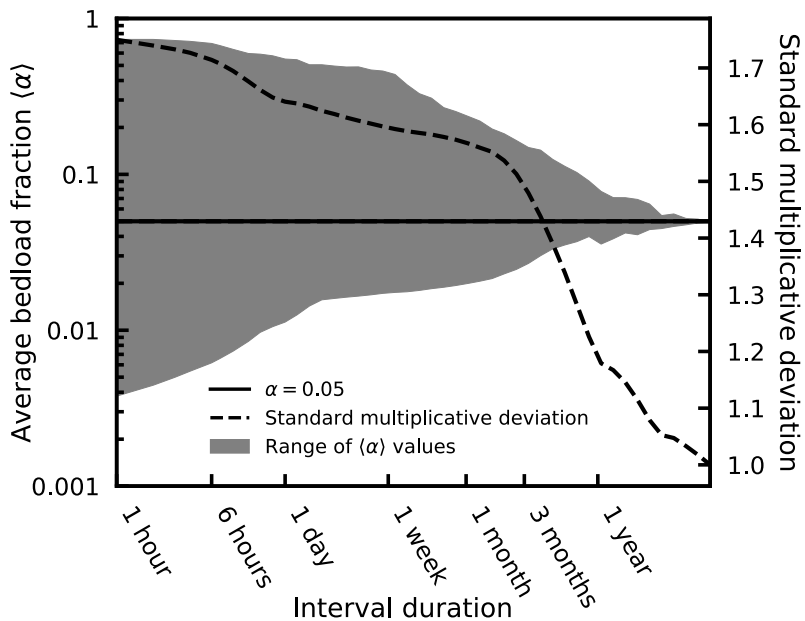


**Figure 14.** Plot illustrating the timescale dependence of the average bedload fraction,  $\langle\alpha\rangle$ . Average bedload fraction was computed for every period with the duration indicated on the x axis. The filled gray area spans the full range of average bedload fractions computed for intervals with the specified duration. The dotted gray line shows the standard deviation of the average bedload fraction as a function of interval duration. At the minimum model resolution, bedload fraction may range from 0.004 to 0.74.

[2013]), we find that cumulative bedload discharge was approximately 5% of the cumulative suspended sand discharge over the nine-year record considered here. However, instantaneous bedload flux ranges from less than 1% to as much as 75% of suspended sand load depending on water discharge and the supply-limitation state. As a result, short-term mass-balance fluctuations caused by experimental changes in discharge regime (i.e. controlled floods), transient accommodation of tributary sand pulses, or prolonged periods of constant discharge are not adequately represented using a constant bedload fraction or rating curve model for bedload flux. For example, cumulative bedload during controlled floods is only 2% of cumulative suspended load during the same intervals, whereas the cumulative bedload is 10% of cumulative suspended load during period when flow is below the mean annual discharge. In general, the magnitude of deviations in short-term average bedload fraction from a measured long-term average is a function of averaging timescale (Figure 14)

Over longer timescales, researchers aim to constrain the effects of changes in the water discharge or sediment delivery regime as dictated by dam protocols, climate, and land use in the upper Colorado River basin [e.g., Andrews, 1991; Grams *et al.*, 2013; Mueller *et al.*, 2014; Grams *et al.*, 2015; Kasprak *et al.*, 2018; Mueller *et al.*, 2018]. In particular, the dam-regulated water discharge regime is the primary tool for enacting management decisions aimed at balancing ecological, social, and economic goals. Nearly three decades of Grand Canyon research suggests that a return to a more natural, seasonal discharge regime would induce a desirable geomorphic response. Actionable proposals like the “Fill Mead First” plan [Schmidt *et al.*, 2016] are designed to balance this and other management objectives by changing the annual cycle of dam releases, and flux-based sediment budgets are critical for accurately evaluating the effects and effectiveness of such plans. However, the intended geomorphic response will necessarily involve changes in channel geometry and bed composition, affecting sediment flux in a manner that cannot be tracked using

704 traditional rating curve or bedload fraction approaches. Measurements of  $q_w$ ,  $C_s$  and  $D_s$   
 705 are indicative of changes in  $q_b$  and such that it is possible to resolve short-term morpho-  
 706 dynamic adjustment and evaluate the effects of future changes in the water discharge and  
 707 sediment supply regime.

#### 708 5.4 Other applications of modeling approach

709 Bedload has historically been difficult to measure directly. As a result, its role in  
 710 governing large-scale river organization poorly understood. Although this paper focuses  
 711 on estimating bedload on the Colorado River, the modeling approach presented herein will  
 712 enable improved estimates of bedload flux in any sand-bedded river. Our model can be  
 713 applied retroactively to innumerable historical measurements of suspended sediment con-  
 714 centration and grain size, providing a new approach for connecting bedload transport to  
 715 continent- and basin-scale river dynamics.

716 This work also supports a more general principle that extends beyond the problem  
 717 of estimating bedload flux. We have argued that our bedload model provides reliable pre-  
 718 dictions because it approximates quasi-universal relationships between transport param-  
 719 eters emerge through the processes governing their interaction and equilibration. In this  
 720 view, first order changes in flow and transport conditions including bedload flux, sus-  
 721 pended sand concentration, and suspended sand diameter are driven by three variables:  
 722 water discharge, slope, and bed material grain size. This implies that any relevant variable  
 723 can be estimated from measurements of three other variables, providing a general formula  
 724 for constructing predictive empirical relations in sandy fluvial systems. This strategy may  
 725 prove useful for reconstructing hydraulic and transport conditions in scenarios where cer-  
 726 tain variables are difficult or impossible to measure, for example in applications involving  
 727 remotely sensed river data or measurements of fluvial sedimentary rocks.

## 728 6 Conclusions

729 The modeling approach presented here was developed to estimate reach-averaged  
 730 bedload flux from measurements of water discharge, concentration, and grain size in sus-  
 731 pension. This approach is based on the assumption that most of the variability in sand-bed  
 732 rivers can be reduced to three principle modes of variation that are causally attributed to  
 733 water discharge, slope, and bed grain size. Measurements of concentration and grain size  
 734 in suspension provide reliable proxies for the effect of slope and bed material grain size  
 735 on bedload flux.

736 Bayesian hierarchical modeling assumes similarity between rivers to ensure efficient  
 737 use of limited data. This approach reduces in-sample bias compared with a fully grouped  
 738 regression, and it improves parameter estimation precision compared with the ungrouped  
 739 regression. However, we anticipate that the general modeling approach presented here may  
 740 prove useful in other contexts for which grouped or ungrouped generative data models  
 741 may be preferable.

742 We find that predicted bedload flux during the period from 2008 to 2016 averaged  
 743 over the full gage record at Diamond Creek is approximately 5% of the measured sus-  
 744 pended sediment load. However, instantaneous values deviate significantly from 5% de-  
 745 pending on flow strength and sediment supply conditions. Notably, changes in bedload  
 746 flux at a constant water discharge are indicative of short-term sediment supply enrichment  
 747 and depletion. Using the median prediction from the hierarchical model, we find that bed-  
 748 load flux ranges from as high as 75 % of suspended sand load (during fine-sand depleted,  
 749 low-discharge periods) to less than 1% (during fine-sand enriched floods). The decade-  
 750 average bedload fraction is expected to deviate systematically from 5% in the future if bed  
 751 composition and channel geometry evolve due to changes in tributary sand supply or the  
 752 dam-regulated discharge regime. In order to ensure accurate quantification of fluctuations

753 in sediment storage over a range of timescales, it is critical to account for deviations in  
 754 the ratio of bedload to suspended load driven both by individual events (for example, high  
 755 flow experiments or tributary floods) and long-term evolution of channel geometry and  
 756 bed composition.

#### 757 **A: Estimating bedload flux from repeat bathymetric surveys of dune migration**

758 Bedload flux estimates at our site were computed from point clouds of bed topog-  
 759 raphy obtained at approximately six-minute intervals. This was accomplished using the  
 760 following procedure:

- 761 1. Flow direction is determined by inspection and point clouds are transformed to  
 762 streamwise and cross-stream coordinates.
- 763 2. An upstream and downstream extent is chosen to bracket a region of the bed used  
 764 for computation of flux. The region used here is largest region where the margins  
 765 of the bedform field are parallel and bedform geometry appears to be uniform in all  
 766 surveys.
- 767 3. Point clouds are divided by cross-stream coordinate into streamwise oriented tran-  
 768 sects spaced at 25 cm.
- 769 4. Ungridded points that fall within each 25 cm-wide transect are gridded at a 10 cm  
 770 streamwise resolution using a locally-weighted nonparametric filter.
- 771 5. Transects are detrended using a high-pass Fourier filter. The filter wavelength used  
 772 here is three times the largest dune length determined by inspection.
- 773 6. Characteristic bedform height is estimated as  $2\sqrt{2} * \sigma_\eta$  where  $\sigma_\eta$  is the root mean  
 774 squared detrended bed elevation [McElroy, 2009]
- 775 7. A matrix of dune displacements (determined from the maximum of the cross-correlation  
 776 function) is computed for each transect using every pair of surveys. Valid displace-  
 777 ments are retained to calculate migration rate according to the following criteria:  
 778 (a) temporal separation is not greater than one hour, (b) displacement is not greater  
 779 than 20 percent of the bedform length, determined from the spectral centroid of  
 780 the detrended bed profile [Van der Mark & Blom, 2007], (c) the maximum of the  
 781 cross correlation function is not less than 0.8, and (d) the implied migration rate  
 782 (displacement divided by temporal separation) is not greater than 3 meters per hour  
 783 and not less than 0.3 meters per hour. These criteria optimize temporal resolution  
 784 and stability of the bedload flux calculation, and reliably discriminate transects with  
 785 active dune evolution from plane-bed topography.
- 786 8. Bedform migration rate is computed for each transect using ordinary least-squares  
 787 regression forced through the origin with all valid displacements.
- 788 9. Volumetric bedload flux per unit width is computed for each streamwise transect  
 789 using the bedform bedload equation [Simons *et al.*, 1965].
- 790 10. Total bedload mass flux was computed for each transect by multiplying unit bed-  
 791 load flux by the transect width (25 cm) and the density of quartz (2650 kg/m<sup>3</sup>),  
 792 then summed.

793 We find that the bedform migration rate regression using displacements forward and back-  
 794 ward in time is necessary to ensure stable results. However, this means that bedload flux  
 795 estimates are derived from overlapping data. Down sampling is thus necessary to ensure  
 796 that each reported value of bedload flux is computationally independent: we consider a  
 797 maximum temporal resolution of one hour. Results are plotted in Figure 4.

#### 798 **B: Bayesian regression**

799 Here, we provide additional details on the statistical techniques employed in this pa-  
 800 per. In order to make this explanation more clear, we adopt notation that is common in

statistical literature [e.g. *Gelman et al.*, 1995; *Christensen et al.*, 2011]. We consider the problem of predicting a continuous response variable  $y$  from a vector of predictor variables  $\bar{\mathbf{x}} = [1, x_1, x_2, x_3]$ . The relationship between predictor variables and response variables is studied using a probabilistic model with parameters  $\theta$  for the data generating process.

Physical variables of interest are log-transformed and normalized to obtain linear predictor and response variables such that  $y = \log(q_b/q_{b0})$ ,  $x_1 = \log(Q/Q_0)$ ,  $x_2 = \log(C_s/C_{s0})$  and  $x_3 = \log(D_s/D_{s0})$  and The subscript 0 denotes the geometric mean of all observations, which is equivalent to subtracting the arithmetic mean of log-transformed variables and results in centered response and predictor variables. This is a convention that facilitates interpretation of the intercept term  $\beta_0$ . The subscript  $i$  denotes a specific observation such that  $y_i$  and  $\bar{\mathbf{x}}_i$  are the  $i^{th}$  of  $n$  observations of response and predictor variables, respectively. A capital  $X$  is short hand for all observations of model variables, i.e.  $X = (\bar{\mathbf{x}}_0, \dots, \bar{\mathbf{x}}_n, y_0, \dots, y_n)$ . Finally, we use  $\tilde{\mathbf{x}}_i$  to denote a vector of observations of predictor variables for which we intend to predict an unobserved value of the response variable,  $\tilde{y}_i$ .

### B.1 Grouped model

The grouped model ignores potential correlations that may exist on a site specific basis. All data is pooled into a single normal linear regression analysis. Regression coefficients and errors are assumed to be equivalent at all sites. Here,  $\boldsymbol{\beta} = [\beta_0, \beta_1, \beta_2, \beta_3]$  is a  $1 \times 4$  vector of regression coefficients. The  $i^{th}$  observation of the response variable  $y_i$  is modeled as a linear function of predictor variables plus a normally-distributed independent error term (e.g. equation 8). This is equivalent to specifying that the  $y_i$  follows a normal distribution with mean  $\boldsymbol{\beta}\bar{\mathbf{x}}_i$  and standard deviation  $\sigma$ . Formally, the probability of observing  $y_i$  given  $\bar{\mathbf{x}}_i$ ,  $\boldsymbol{\beta}$ , and  $\sigma$  is given by:

$$p(y_i|\bar{\mathbf{x}}_i, \boldsymbol{\beta}, \sigma) = \frac{1}{\sqrt{2\pi\sigma^2}} \exp\left[-\frac{(y_i - \boldsymbol{\beta}\bar{\mathbf{x}}_i)^2}{2\sigma^2}\right] \quad (\text{B.1})$$

and the likelihood of model parameters  $\theta = (\boldsymbol{\beta}, \sigma)$  conditional on all observational data  $X = (x_0, \dots, x_n, y_0, \dots, y_n)$  is simply the product of the probabilities of each individual observation:

$$L(\theta|X) = \prod_{i=1}^n p(y_i|\bar{\mathbf{x}}_i, \boldsymbol{\beta}, \sigma). \quad (\text{B.2})$$

For the grouped model, we employ the following independent priors for model parameters:

$$\beta_0 \sim \mathcal{N}(0, 100) \quad (\text{B.3})$$

$$\beta_1 \sim \mathcal{N}(0, 100) \quad (\text{B.4})$$

$$\beta_2 \sim \mathcal{N}(0, 100) \quad (\text{B.5})$$

$$\beta_3 \sim \mathcal{N}(0, 100) \quad (\text{B.6})$$

$$\sigma \sim \Gamma^{-1}(0.001, 0.001). \quad (\text{B.7})$$

Here,  $\mathcal{N}(\mu, \sigma)$  denotes a normal distribution with mean  $\mu$  and standard deviation  $\sigma$ , and  $\Gamma^{-1}(\alpha_1, \alpha_2)$  denotes the inverse gamma distribution with shape parameter  $\alpha_1$  and scale parameter  $\alpha_2$ . Since the marginal priors are independent,  $p(\boldsymbol{\beta}, \sigma) = p(\beta_0)p(\beta_1)p(\beta_2)p(\beta_3)p(\sigma)$ . These priors approximate Jeffrey's prior for normal linear regression which is a uniform distribution on  $(\boldsymbol{\beta}, \log(\sigma))$  [*Gelman et al.*, 1995; *Christensen et al.*, 2011].

The posterior probability distribution of model parameters  $\theta$  given data  $X$  is proportional to the product of the likelihood function and the prior:

$$P(\theta|X) = \frac{L(\theta|X)P(\theta)}{\int L(\theta|X)P(\theta)d\theta}, \quad (\text{B.8})$$

where the constant of proportionality  $[\int L(\theta|X)P(\theta)d\theta]^{-1}$  ensures that the posterior integrates to 1.

## B.2 Ungrouped model

The ungrouped model involves fitting separate regression models for each site. Henceforth, the subscript  $j = 1, \dots, m$  denotes the  $j^{th}$  of  $m = 8$  sites.  $\beta_j = [\beta_{0j}, \beta_{1j}, \beta_{2j}, \beta_{3j}]$  is thus the vector of regression coefficients corresponding to site  $j$ , and  $\sigma_j$  is the standard deviation of the error term at site  $j$ . The full data model thus contains  $4 \times m$  regression coefficients and  $m$  error terms, totaling 40 parameters compared with the 5 parameters used in the ungrouped model.

Each site has a different number of observations,  $n_j$ . The probability of observing  $i^{th}$  of  $n_j$  observations of the response variable at site  $j$ ,  $y_{i,j}$  given  $x_{i,j}$ ,  $\beta_j$ , and  $\sigma_j$  is given by

$$p(y_{i,j}|x_{i,j}, \beta_j, \sigma_j) = \frac{1}{\sqrt{2\pi\sigma_j^2}} \exp\left[-\frac{(y_{i,j} - \beta_j x_{i,j})^2}{2\sigma_j^2}\right] \quad (\text{B.9})$$

and the likelihood function of model parameters  $\theta = (\beta_0, \dots, \beta_m, \sigma_0, \dots, \sigma_m)$  conditional on all observational data  $X$  is given by the product of the probabilities of all observations:

$$L(\theta|X) = \prod_{j=1}^m \prod_{i=1}^{n_j} (y_{i,j}|x_{i,j}, \beta_j, \sigma_j) \quad (\text{B.10})$$

Separate independent priors are used for each site, i.e.:

$$\beta_{0j} \sim N(0, 100) \quad (\text{B.11})$$

$$\beta_{1j} \sim N(0, 100) \quad (\text{B.12})$$

$$\beta_{2j} \sim N(0, 100) \quad (\text{B.13})$$

$$\beta_{3j} \sim N(0, 100) \quad (\text{B.14})$$

$$\sigma_j \sim \Gamma^{-1}(0.001, 0.001). \quad (\text{B.15})$$

## B.3 Hierarchical Model

Like the ungrouped model, the hierarchical model involves fitting separate regression coefficients for each site. However, unlike the ungrouped model, these regression coefficients are assumed to come from a common distribution that encompasses the range of parameters that exist in sand bed rivers. Additionally, there is a single error term  $\sigma$  applied at all sites. Instead of using separate, diffuse priors with fixed parameters for the regression coefficients at each site, informative, dynamic priors are used, i.e.:

$$\beta_{0j} \sim N(\mu_{\beta_0}, \varsigma_{\beta_0}) \quad (\text{B.16})$$

$$\beta_{1j} \sim N(\mu_{\beta_1}, \varsigma_{\beta_1}) \quad (\text{B.17})$$

$$\beta_{2j} \sim N(\mu_{\beta_2}, \varsigma_{\beta_2}) \quad (\text{B.18})$$

$$\beta_{3j} \sim N(\mu_{\beta_3}, \varsigma_{\beta_3}) \quad (\text{B.19})$$

$$\sigma \sim \Gamma^{-1}(0.001, 0.001). \quad (\text{B.20})$$

Here,  $\psi = (\mu_{\beta_0}, \mu_{\beta_1}, \mu_{\beta_2}, \mu_{\beta_3}, \varsigma_{\beta_0}, \varsigma_{\beta_1}, \varsigma_{\beta_2}, \varsigma_{\beta_3})$  are known as hyperparameters;  $\mu$  terms are the mean of the prior on the regression coefficients and represent the central tendency of sites in our data set (as a proxy for sand bed rivers), while  $\varsigma$  terms are the standard deviation of the priors and represent the variability present across sites in our dataset. Because

864 the priors depend on dynamic hyperparameters, the posterior probability takes a slightly  
 865 different form:

$$p(\theta|X) = \frac{L(\theta|X)P(\theta|\psi)P(\psi)}{\int[L(\theta|X)P(\theta|\psi)P(\psi)]d\theta d\psi}, \quad (\text{B.21})$$

866 where  $P(\theta|\psi)$  is the prior probability distribution for model parameters  $\theta$  given hyperpa-  
 867 rameters  $\psi$ , and  $P(\psi)$  is the prior probability distribution for  $\psi$ , or the hyperprior. Re-  
 868 ported results were obtained using the following diffuse, independent hyperpriors:

$$\mu_k \sim \mathcal{N}(0, 100) \quad (\text{B.22})$$

$$\varsigma_k \sim \Gamma^{-1}(0.001, 0.001) \quad (\text{B.23})$$

869 for  $k = 0, 1, 2, 3$ . The grouped and ungrouped models can be framed as special cases of  
 870 the hierarchical model with informative hyperpriors. Specifically, the grouped model is a  
 871 case where  $\varsigma_k \sim \delta(0)$ , where  $\delta$  is the dirac delta function. This leads to  $\beta_k = \mu_k$  for  
 872 all sites. The ungrouped model is a case where  $\mu_k \sim \delta(0)$  and  $\varsigma_k \sim \delta(100)$  such that the  
 873 hyperpriors exert minimal influence on  $\beta_k$ .

#### B.4 MCMC sampling

874 Posterior distributions for model parameters were constructed using the No-U-Turn  
 875 sampling (NUTS) algorithm [Hoffman & Gelman, 2014], as implemented in the open  
 876 source Python package, PyMC3 [Salvatier et al., 2016]. The sampler was initiated us-  
 877 ing the automatic differentiation variational inference algorithm [Kucukelbir et al., 2016].  
 878 Three chains were used, and 1000 burn-in steps were more than sufficient to achieve con-  
 879 vergence. The posterior distribution of model parameters was approximated using 5000  
 880 steps without thinning.

#### B.5 Prediction

881 Once the posterior probability distribution of model parameters is known, unob-  
 882 served values of the response variable  $\tilde{y}_i$  can be estimated using Bayesian posterior pre-  
 883 dictive distributions. The posterior predictive density  $P(\tilde{y}_i|\tilde{x}_i, X)$  is found by integrating  
 884 the sampling distribution of  $\tilde{y}_i$  given a specific set of parameters,  $p(\tilde{y}_i|\tilde{x}_i, \theta)$ , against the  
 885 posterior distribution of model parameters,  $P(\theta|X)$ :

$$P(\tilde{y}_i|\tilde{x}_i, X) = \int P(\tilde{y}_i|\tilde{x}_i, \theta)P(\theta|X)d\theta. \quad (\text{B.24})$$

886 This distribution is straightforward to compute numerically using MCMC techniques.  
 887 In addition to predicting single unobserved values of  $q_b$ , it is possible to obtain a simu-  
 888 lated predictive distribution for any conceivable quantity that can be expressed as a func-  
 889 tion of model parameters (for example, time-integrated bedload flux).

#### B.6 Deviance Information Criterion

890 The Deviance Information Criterion (DIC) is a measure of relative predictive power  
 891 that reflects the trade-off between goodness of fit and parameter estimation precision [Spiegel-  
 892 halter et al., 2002; Gelman et al., 2014]. It is used here instead of other more well-known  
 893 model selection criteria like the Akaike information criterion (AIC) or the Bayesian in-  
 894 formation criterion (BIC) because unlike AIC, it is suitable for comparing the hierarchi-  
 895 cal and non-hierarchical models considered here, and unlike BIC, its intended use is for  
 896 comparing expected out-of-sample predictive accuracy under the assumption that the data  
 897 model is correct.

901 DIC uses the log-likelihood  $\log L(\theta|X)$  of different models to compare expected out  
 902 of sample predictive accuracy. Models that achieve higher values of the likelihood func-

903 tion provide better in-sample fit. The log-likelihood of the posterior mean parameter esti-  
 904 mate  $\log L(\bar{\theta}|X)$  is used here to quantify model fit. For clarity,  $\bar{\theta} = E(\theta|X)$  is the posterior  
 905 mean parameter estimate.

906 More complex models may lead to higher log-posterior densities and better in-sample  
 907 fit at the cost of parameter estimation precision. In other words, a much wider range of  
 908 model parameters provide a good fit to the data such that it is difficult to select optimal  
 909 values. For models that are too complex, predictive uncertainty is primarily related to un-  
 910 certainty in model parameters rather than being directly quantified by the noise term ( $\sigma$   
 911 in the models presented here). It is thus necessary to introduce a correction factor that  
 912 accounts for parameter estimation uncertainty. Here, the effective number of parameters  
 913  $p_{DIC} = 2\text{var}_{post}(\log L(\theta|X))$  is framed in terms of the posterior variance in the log-  
 914 likelihood, and can be computed by taking the variance of MCMC sampled log-likelihoods.

915 The expected log predictive density is given by  $\text{elpd} = \log L(\bar{\theta}|X) - p_{DIC}$ . Assuming  
 916 predictive error is normally distributed, the expected log predictive density is proportional  
 917 to the mean squared error. DIC is a related to the expected log posterior density by a fac-  
 918 tor of -2 due to convention:

$$DIC = -2 \log L(\bar{\theta}|X) + 2p_{DIC} \quad (\text{B.25})$$

919 For additional details on the derivation and interpretation of DIC, see *Spiegelhalter*  
 920 *et al.* [2002]; Gelman *et al.* [2014].

## 921 Acknowledgments

922 We thank Bob Tusso, Dan Hamill, and Erich Mueller their help in the field. U.S. Geo-  
 923 logical Survey studies in Grand Canyon are supported by the Grand Canyon Dam Adap-  
 924 tive Management Program administered by the U.S. Department of the Interior Bureau of  
 925 Reclamation. Additional support was provided by the University of Wyoming School of  
 926 Energy Resources. Data and software supporting the analysis and conclusions presented  
 927 here are available online through the SEAD data repository and github [Leary, 2018; Ash-  
 928 ley, 2019a,b]. Any use of trade, product, or firm names is for descriptive purposes only  
 929 and does not imply endorsement by the U.S. Government.

## 930 References

- 931 Ashley, T. (2019) qDune version 1.0 [Computer Software]  
 932 <https://doi.org/10.5281/zenodo.3515483>
- 933 Ashley, T. (2019) qbStats version 1.0 [Computer Software]  
 934 <https://doi.org/10.5281/zenodo.3515485>
- 935 Andrews, E. D. (1991). Sediment transport in the Colorado River basin. In *Colorado River*  
 936 *Ecology and Dam Management: Proceedings of a Symposium* (pp. 54–74). Washington,  
 937 DC: National Academies Press.
- 938 Brownlie, W. R. (1983). Flow depth in sand-bed channels. *Journal of Hydraulic Engineer-  
 939 ing*, 109(7), 959–990.
- 940 Buscombe, D., Rubin, D. M., & Warrick, J. A. (2010). A universal approximation of grain  
 941 size from images of noncohesive sediment. *Journal of Geophysical Research: Earth Sur-  
 942 face*, 115, F02015. <https://doi.org/10.1029/2009JF001477>
- 943 Buscombe, D., Grams, P. E., & Kaplinski, M. A. (2014a). Characterizing riverbed  
 944 sediment using high-frequency acoustics: 1. Spectral properties of scat-  
 945 tering. *Journal of Geophysical Research: Earth Surface*, 119, 2674–2691.  
 946 <https://doi.org/10.1002/2014JF003189>
- 947 Buscombe, D., Grams, P. E., & Kaplinski, M. A. (2014b). Characterizing riverbed sed-  
 948 iment using high-frequency acoustics: 2. Scattering signatures of Colorado Riverbed

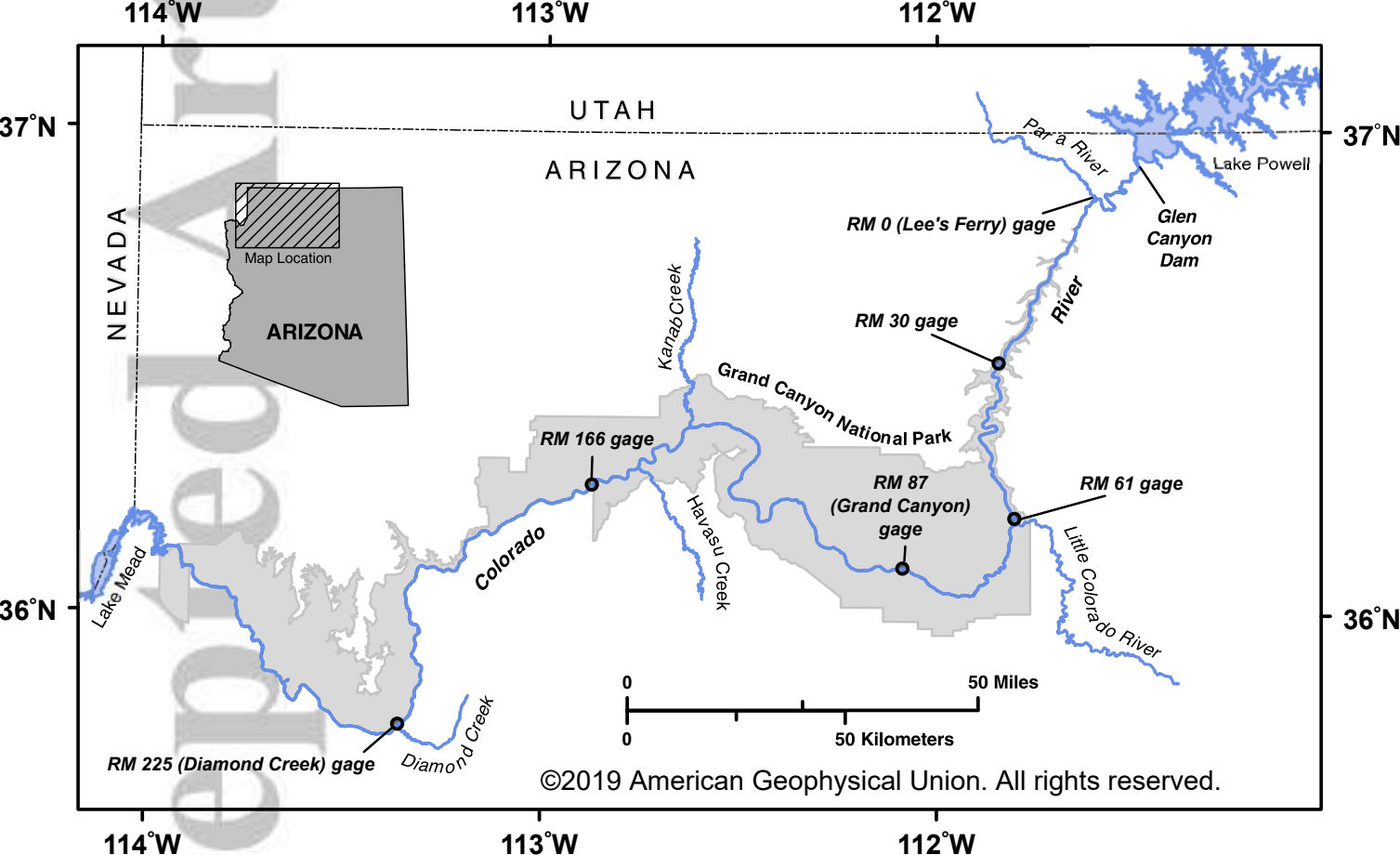
- 949 sediment in Marble and Grand Canyons. *Journal of Geophysical Research: Earth Surface*, 119, 2692–2710. <https://doi.org/10.1002/2014JF003191>
- 950
- 951 Christensen, R., Johnson, W., Branscum, A., & Hanson, T. E. (2011). *Bayesian ideas and*  
952 *data analysis: An introduction for scientists and statisticians*. Boca Raton, FL: Chapman  
953 Hall.
- 954 Dean, D. J., Topping, D. J., Schmidt, J. C., Griffiths, R. E., & Sabol, T. A., (2016). Sediment  
955 supply versus local hydraulic controls on sediment transport and storage in a river  
956 with large sediment loads, *Journal of Geophysical Research: Earth Surface* 121, 82–110,  
957 <https://doi.org/10.1002/2015JF003436>.
- 958 Dolan, R., Howard, A., & Gallenson., A. (1974), Man's impact on the Colorado River  
959 in the Grand Canyon: The Grand Canyon is being affected both by the vastly changed  
960 Colorado River and by the increased presence of man. *American Scientist*, 62(4), 392–  
961 401.
- 962 Einstein, H. A. (1950). The bed load function in open channel flows. *U.S. Dept. of Agriculture Technical Bulletin No. 1026*.
- 963
- 964 Einstein, H. A., & Chien, N. (1953). Can the rate of wash load be predicted from the  
965 bedload function?. *Eos, Transactions American Geophysical Union*, 34(6), 876-882.
- 966 Ellison, C. A., Groten, J. T., Lorenz, D. L., & Koller, K. S. (2016). Application of dimensionless  
967 sediment rating curves to predict suspended-sediment concentrations, bedload,  
968 and annual sediment loads for rivers in Minnesota. *USGS Scientific Investigations Report*  
969 *No. 2016-5146*.
- 970 Emmett, W. W., & Wolman, M. G. (2001). Effective discharge and gravel-  
971 bed rivers. *Earth Surface Processes and Landforms*, 26(13), 1369–1380.  
972 <https://doi.org/10.1002/esp.303>
- 973 Engel, P., and Lau, Y. L. (1980), Computation of bed load using bathymetric data. *Journal*  
974 *of the Hydraulics Division of the American Society of Civil Engineers*, 106(HY3), 369–380.
- 975
- 976 Engelund, F., & Hansen, E. (1967). A monograph on sediment transport in alluvial  
977 streams. *Technisk Forlag, Copenhagen, Denmark*.
- 978 Gaeuman, D., & Jacobson, R. B. (2007). Field assessment of alternative bed-load trans-  
979 port estimators. *Journal of Hydraulic Engineering*, 133(12), 1319-1328.
- 980 Garcia, M. (2008). Sediment transport and morphodynamics. In *Sedimentation Engineer-  
981 ing: Process, Management, Modeling and Practice* (pp. 21–163). Reston, VA: ASCE.
- 982 Garcia, M., & Parker, G. (1991). Entrainment of bed sediment into suspension. *Journal of  
983 Hydraulic Engineering*, 117(4), 414–435.
- 984 Gelman, A., Carlin, J. B., Stern, H. S., Dunson, D. B., Vehtari, A., & Rubin, D. B.  
985 (1995). *Bayesian data analysis*. Chapman and Hall/CRC.
- 986 Gelman, A., Hwang, J., & Vehtari, A. (2014). Understanding predictive informa-  
987 tion criteria for Bayesian models. *Statistics and computing*, 24(6), 997–1016.  
988 <https://doi.org/10.1007/s11222-013-9416-2>
- 989 Gibbings, J. C. (2011). The Pi-Theorem. In *Dimensional Analysis* (pp. 55-82). Springer,  
990 London.
- 991 Grams, P. E., Topping, D. J., Schmidt, J. C., Hazel, J. E., & Kaplinski, M. (2013). Linking  
992 morphodynamic response with sediment mass balance on the Colorado River in Marble  
993 Canyon: Issues of scale, geomorphic setting, and sampling design. *Journal of Geophysi-  
994 cal Research: Earth Surface*, 118(2), 361–381. <https://doi.org/doi:10.1002/jgrf.20050>
- 995 Grams, P. E., Schmidt, J. C., Wright, S. A., Topping, D. J., Melis, T. S., & Rubin, D. M.  
996 (2015). Building sandbars in the Grand Canyon. *EOS: Transactions of the American  
997 Geophysical Union*, 96, 1–11. <https://doi.org/doi:10.1002/jgrf.20050>
- 998 Grams, P. E., Buscombe, D., Topping, D. J., Kaplinski, M., & Hazel, J. E. (2018). How  
999 many measurements are required to construct an accurate sand budget in a large river?  
1000 Insights from analyses of signal and noise. *Earth Surface Processes and Landforms*, 44,  
1001 160–178. <https://doi.org/10.1002/esp.4489>

- 1002 Gray, J. R., Gartner, J. W., Barton, J. S., Gaskin, J., Pittman, S. A., & Rennie, C. D.  
 1003 (2010). Surrogate technologies for monitoring bed-load transport in rivers. *Sedimentology of Aqueous Systems*, 2, 45–79.
- 1004  
 1005 Gray, J. R., & Gartner, J. W. (2009). Technological advances in suspended-  
 1006 sediment surrogate monitoring. *Water resources research*, 45(4).  
 1007 <https://doi.org/10.1029/2008WR007063>
- 1008 Hastie, T., Tibshirani, R., & Friedman, J. H. (2009). Model assessment and selection. In  
 1009 *The Elements of Statistical Learning: Data Mining, Inference, and Prediction*, (pp. 219–  
 1010 260). New York, NY: Springer.
- 1011 Hoffman, M. D., & Gelman, A. (2014). The No-U-turn sampler: adaptively setting path  
 1012 lengths in Hamiltonian Monte Carlo. *Journal of Machine Learning Research*, 15(1),  
 1013 1593–1623. <https://arxiv.org/pdf/1111.4246>
- 1014 Holmes, R. R. (2010). Measurement of bedload transport in sand-bed rivers: A look at  
 1015 two indirect sampling methods. *US Geological Survey Scientific Investigations Report*,  
 1016 5091, 236–252.
- 1017 Ingram, H., Tarlock, A. D., & Oggins, C. R. (1991). The law and politics of the operation  
 1018 of Glen Canyon Dam. In *Colorado River Ecology and Dam Management: Proceedings of*  
 1019 *a Symposium* (pp. 10–27), Washington, DC: National Academies Press.
- 1020 Minckley, W. L. (1991). Native fishes of the Grand Canyon region: an obituary. In *Col-  
 1021 orado River Ecology and Dam Management: Proceedings of a Symposium* (pp. 124–177),  
 1022 Washington, DC: National Academies Press.
- 1023 Kaplinski, M., Hazel, J. E., Parnell, R., Breedlove, M., Kohl, K., & Gonzales, M. (2009).  
 1024 Monitoring fine-sediment volume in the Colorado River ecosystem, Arizona; Bathymet-  
 1025 ric survey techniques *U.S. Geological Survey Open-File Report 2009-1207*.
- 1026 Kaplinski, M., Hazel Jr, J. E., Grams, P. E., & Davis, P. A. (2014). Monitoring fine-  
 1027 sediment volume in the Colorado River ecosystem, Arizona: Construction and anal-  
 1028 ysis of digital elevation models *U.S. Geological Survey Open-File Report 2014-1052*.  
 1029 <https://dx.doi.org/10.3133/ofr20141052>
- 1030 Kasprak, A., Sankey, J. B., Buscombe, D., Caster, J., East, A. E., & Grams, P. E. (2018).  
 1031 Quantifying and forecasting changes in the areal extent of river valley sediment in re-  
 1032 sponse to altered hydrology and land cover *Progress in Physical Geography: Earth and*  
 1033 *Environment*, 42(6). 739–764. <https://doi.org/10.1177/0309133318795846>
- 1034 Kucukelbir, A., Tran, D., Ranganath, R., Gelman, A., & Blei, D. M. (2017). Automatic  
 1035 differentiation variational inference. *The Journal of Machine Learning Research*, 18(1),  
 1036 430–474. <https://arxiv.org/pdf/1603.00788.pdf>
- 1037 Leary, K. (2018). Diamond Creek Repeat Multibeam Data, *SEAD Internal Repository*,  
 1038 <http://doi.org/10.5967/M02J6904>
- 1039 Leopold, L. B., & Maddock, T. (1953). The hydraulic geometry of stream channels and  
 1040 some physiographic implications *U.S. Geological Survey Professional Paper 252*.
- 1041 McElroy, B. J. (2009). Expressions and implications of sediment transport variability in  
 1042 sandy rivers (PhD Dissertation). <http://hdl.handle.net/2152/15117>
- 1043 McLean, S. R. (1992). On the calculation of suspended load for noncohesive  
 1044 sediments. *Journal of Geophysical Research: Oceans*, 97(C4), 5759–5770.  
 1045 <https://doi.org/10.1029/91JC02933>
- 1046 Meyer-Peter, E., & Müller, R. (1948). Formulas for bed-load transport. In *IAHSR 2nd*  
 1047 *meeting*, Stockholm: IAHR.
- 1048 Mohrig, D., & Smith, J. D. (1996). Predicting the migration rates of subaqueous dunes.  
 1049 *Water Resources Research*, 32(10), 3207–3217.
- 1050 Molinas, A., and Wu, B. (2000). Comparison of fractional bed-material load computation  
 1051 methods in sand-bed channels. *Earth Surface Processes and Landforms*, 25, 1045–1068.
- 1052 Mueller, E. R., Grams, P. E., Schmidt, J. C., Hazel, J. E., Alexander, J. S., & Kaplin-  
 1053 ski, M. (2014). The influence of controlled floods on fine sediment storage in de-  
 1054 bris fan-affected canyons of the Colorado River basin. *Geomorphology*, 226, 65–75.  
 1055 <https://doi.org/10.1016/j.geomorph.2014.07.029>

- 1056 Mueller, E. R., Grams, P. E., Hazel, J. E., & Schmidt, J. C. (2018). Variability  
 1057 in eddy sandbar dynamics during two decades of controlled flooding of the  
 1058 Colorado River in the Grand Canyon. *Sedimentary Geology*, 363, 181–199.  
 1059 <https://doi.org/10.1016/j.sedgeo.2017.11.007>
- 1060 Paola, C., & Voller, V. R. (2005). A generalized Exner equation for sediment  
 1061 mass balance. *Journal of Geophysical Research: Earth Surface*, 110(F4).  
 1062 <https://doi.org/10.1029/2004JF000274>
- 1063 Pitlick, J. (1988). Variability of bed load measurement. *Water Resources Research*, 24(1),  
 1064 173–177. <https://doi.org/10.1029/WR024i001p00173>
- 1065 Rantz, S. E., et al. (1982). Measurement and computation of streamflow, U.S. Geological  
 1066 Survey Water Supply Paper 2175.
- 1067 Rubin, D. M., Tate, G. B., Topping, D. J., & Anima, R. A. (2001). Use of rotating side-  
 1068 scan sonar to measure bedload. *Proceedings of the Seventh Federal Interagency Sedimen-*  
 1069 *tation Conference* (pp. 139–144). Reno, NV: U.S. Geological Survey
- 1070 Rubin, D. M., & Topping, D. J. (2001). Quantifying the relative importance of flow  
 1071 regulation and grain size regulation of suspended sediment transport  $\alpha$  and tracking  
 1072 changes in grain size of bed sediment  $\beta$ . *Water Resources Research*, 37(1), 133–146.  
 1073 <https://doi.org/10.1029/2000WR900250>
- 1074 Rubin, D. M., Topping, D. J., Schmidt, J. C., Hazel, J., Kaplinski, M., & Melis, T. S.  
 1075 (2002). Recent sediment studies refute Glen Canyon Dam hypothesis. *Eos, Transactions*  
 1076 *American Geophysical Union*, 83(25), 273–278. <https://doi.org/10.1029/2002EO000191>
- 1077 Salvatier, J., Wiecki, T. V., & Fonnesbeck, C. (2016). Probabilistic programming in Python  
 1078 using PyMC3. *PeerJ Computer Science* 2:e55. <https://doi.org/10.7717/peerj-cs.55>
- 1079 Schmelter, M. L., Hooten, M. B., & Stevens, D. K. (2011). Bayesian sediment transport  
 1080 model for unisize bed load. *Water Resources Research*, 47(11).
- 1081 Schmelter, M. L., & Stevens, D. K. (2012). Traditional and Bayesian statistical models in  
 1082 fluvial sediment transport. *Journal of Hydraulic Engineering*, 139(3), 336–340.
- 1083 Schmelter, M. L., Erwin, S. O., & Wilcock, P. R. (2012). Accounting for uncertainty in  
 1084 cumulative sediment transport using Bayesian statistics. *Geomorphology*, 175, 1–13.
- 1085 Schmelter, M., Wilcock, P., Hooten, M., & Stevens, D. (2015). Multi-fraction Bayesian  
 1086 sediment transport model. *Journal of Marine Science and Engineering*, 3(3), 1066–1092.
- 1087 Schmidt, J. C., and J. B. Graf (1990). Aggradation and degradation of alluvial sand de-  
 1088 posits, 1965 to 1986, Colorado River, Grand Canyon National Park, Arizona, *US Geo-*  
 1089 *logical Survey Professional Paper 1493*.
- 1090 Schmidt, J. C., Kraft, M., Tuzlak, D., and Walker, A. (2016). Fill mead first: A technical  
 1091 assessment. *White Paper No. 1*, Utah State University Quinney College of Natural Re-  
 1092 sources, Center for Colorado River Studies.
- 1093 Shmueli, G. (2010). To explain or to predict?. *Statistical science*, 25(3), 289–310.  
 1094 <https://doi.org/10.1214/10-STS330>
- 1095 Simons, D. B., Richardson, E. V., & Nordin, C. F. (1965). Bedload Equation for Ripples  
 1096 and Dunes. *U.S. Geological Survey Professional Paper 462-H*.
- 1097 Spiegelhalter, D. J., Best, N. G., Carlin, B. P., & Van Der Linde, A. (2002). Bayesian  
 1098 measures of model complexity and fit. *Journal of the Royal Statistical Society: Series*  
 1099 *B (Statistical Methodology)*, 64(4), 583–639. <https://doi.org/10.1111/1467-9868.00353>
- 1100 Toffaletti, F. B. (1968) A procedure for computation of the total river sand discharge and  
 1101 detailed distribution, bed to surface. *Corps of Engineers Committee on Channel Stabi-*  
 1102 *lization Technical report number 5*.
- 1103 Topping, D. J., Rubin, D. M., & Vierra, L. E. (2000). Colorado River sediment transport:  
 1104 1. Natural sediment supply limitation and the influence of Glen Canyon Dam. *Water*  
 1105 *Resources Research*, 36(2), 515–542. <https://doi.org/10.1029/1999WR900285>
- 1106 Topping, D. J., Rubin, D. M., Nelson, J. M., Kinzel, P. J., & Corson, I. C. (2000).  
 1107 Colorado River sediment transport: 2. systematic bed-elevation and grain-size  
 1108 effects of sand supply limitation. *Water Resources Research*, 36(2), 543–570.  
 1109 <https://doi.org/10.1029/1999WR900286>

- 1110 Topping, D. J., Rubin, D. M., Grams, P. E., Griffiths, R. E., Sabol, T. A., Voichick, N. et  
1111 al. (2010). Sediment transport during three controlled-flood experiments on the Col-  
1112 orado River downstream from Glen Canyon Dam, with implications for eddy-sandbar  
1113 deposition in Grand Canyon National Park, *U.S. Geological Survey Open-File Report*  
1114 2010-1128.
- 1115 Topping, D. J., & Wright, S. A. (2016). Long-term continuous acoustical suspended-  
1116 sediment measurements in rivers – Theory, application, bias, and error. *USGS Profes-  
1117 sional Paper 1823*. <https://doi.org/10.3133/pp1823>
- 1118 Topping, D. J., Melis, T. S., Rubin, D. M., & Wright, S. A. (2004). High-resolution mon-  
1119 itoring of suspended-sediment concentration and grain size in the Colorado River in  
1120 Grand Canyon using a laser-acoustic system. In *Proceedings of the Ninth International  
1121 Symposium on River Sedimentation* (pp. 2507–2514). Yichang, China.
- 1122 Topping, D. J., Wright, S. A., Melis, T. S., & Rubin, D. M. (2007). High-resolution mea-  
1123 surements of suspended-sediment concentration and grain size in the Colorado River  
1124 in Grand Canyon using a multi-frequency acoustic system. In *Proceedings of the Tenth  
1125 International Symposium on River Sedimentation* (Vol. 3). Moscow, Russia.
- 1126 Turowski, J. M., Rickenmann, D., & Dadson, S. J. (2010). The partitioning of the total  
1127 sediment load of a river into suspended load and bedload: a review of empirical data.  
1128 *Sedimentology*, 57(4), 1126–1146.
- 1129 van den Berg, J. H. (1987). Bedform migration and bed-load transport in some rivers and  
1130 tidal environments. *Sedimentology*, 34(4), 681–698.
- 1131 van der Mark, C. F., & Blom, A. (2007). A new and widely applicable bedform tracking  
1132 tool. *Technical Report*, University of Twente, Faculty of Engineering Technology, De-  
1133 partment of Water Engineering and Management.
- 1134 van Rijn, L. C. (1984). Sediment transport, part II: Suspended load transport. *Journal  
1135 of Hydraulic Engineering*, 110(11), 1613–1641. [https://doi.org/10.1061/\(ASCE\)0733-9429\(1984\)110:11\(1613\)](https://doi.org/10.1061/(ASCE)0733-9429(1984)110:11(1613))
- 1136 Wong, M., & Parker, G. (2006). Reanalysis and correction of bed-load relation of Meyer-  
1137 Peter and Müller using their own database. *Journal of Hydraulic Engineering*, 132(11),  
1138 1159–1168. [https://doi.org/10.1061/\(ASCE\)0733-9429\(2006\)132:11\(1159\)](https://doi.org/10.1061/(ASCE)0733-9429(2006)132:11(1159))
- 1139 Wright, S. A., & Kaplinski, M. (2011). Flow structures and sandbar dynamics in a canyon  
1140 river during a controlled flood, Colorado River, Arizona. *Journal of Geophysical Re-  
1141 search: Earth Surface*, 116(F1). <https://doi.org/10.1029/2009JF001442>
- 1142 Wright, S., & Parker, G. (2004). Flow resistance and suspended load in sand-bed rivers:  
1143 simplified stratification model. *Journal of Hydraulic Engineering*, 130(8), 796–805.  
1144 [https://doi.org/10.1061/\(ASCE\)0733-9429\(2004\)130:8\(796\)](https://doi.org/10.1061/(ASCE)0733-9429(2004)130:8(796))
- 1145 Wright, S. A., Topping, D. J., Rubin, D. M., & Melis, T. S. (2010). An approach for mod-  
1146 eling sediment budgets in supply-limited rivers. *Water Resources Research*, 46(10).  
1147 <https://doi.org/10.1029/2009WR008600>
- 1148

# Accepted Article



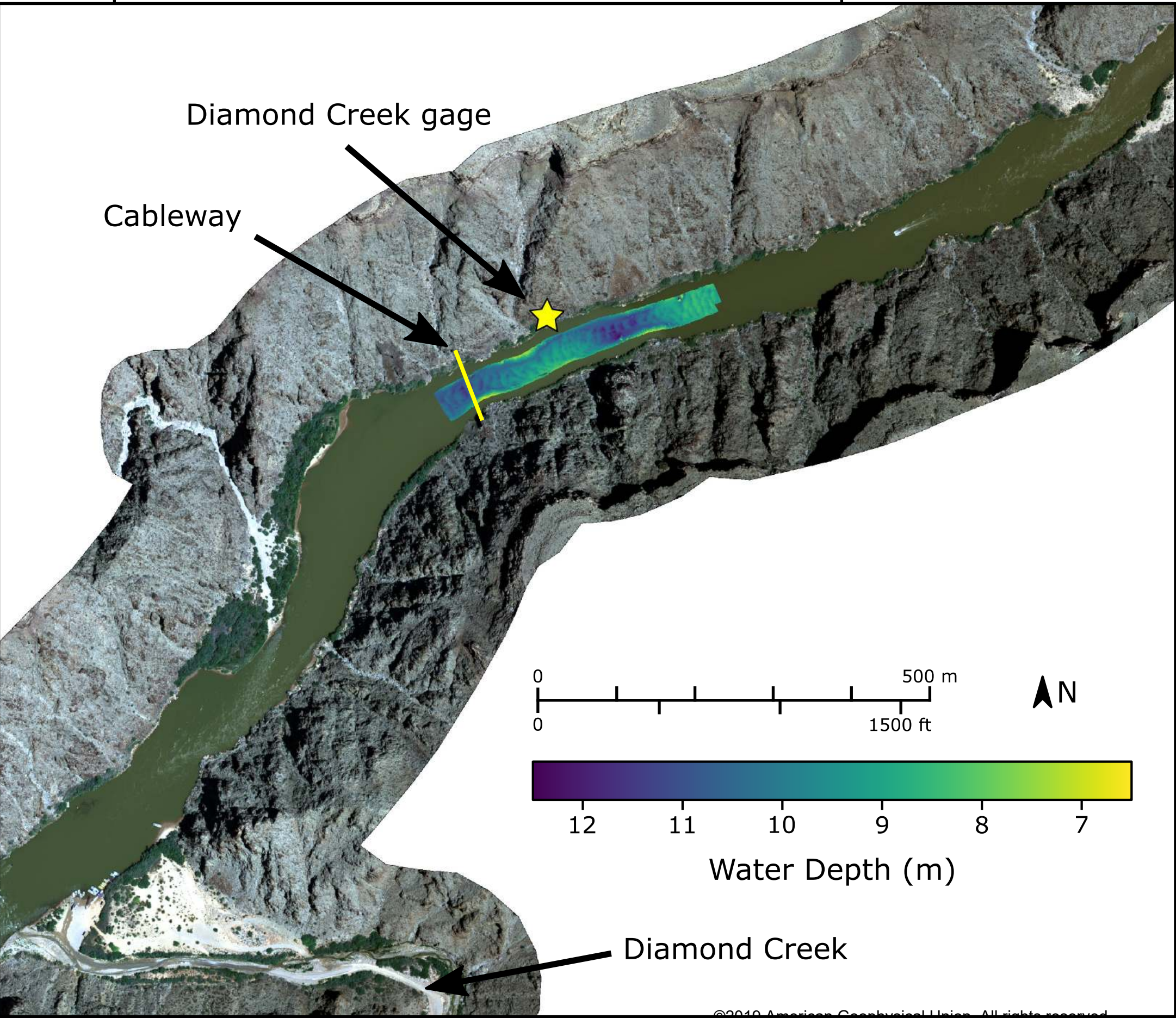
# Accepted Article

113° 22' 21" W

113° 21' 45" W

Diamond Creek gage

Cableway



# Accepted Article

November 11, 2016, 1:15 PM

270 m<sup>3</sup>/s

March 4, 2015, 3:15 PM

380 m<sup>3</sup>/s

July 12, 2015, 8:45 PM

490 m<sup>3</sup>/s

July 12, 2015, 12:00 PM

575 m<sup>3</sup>/s



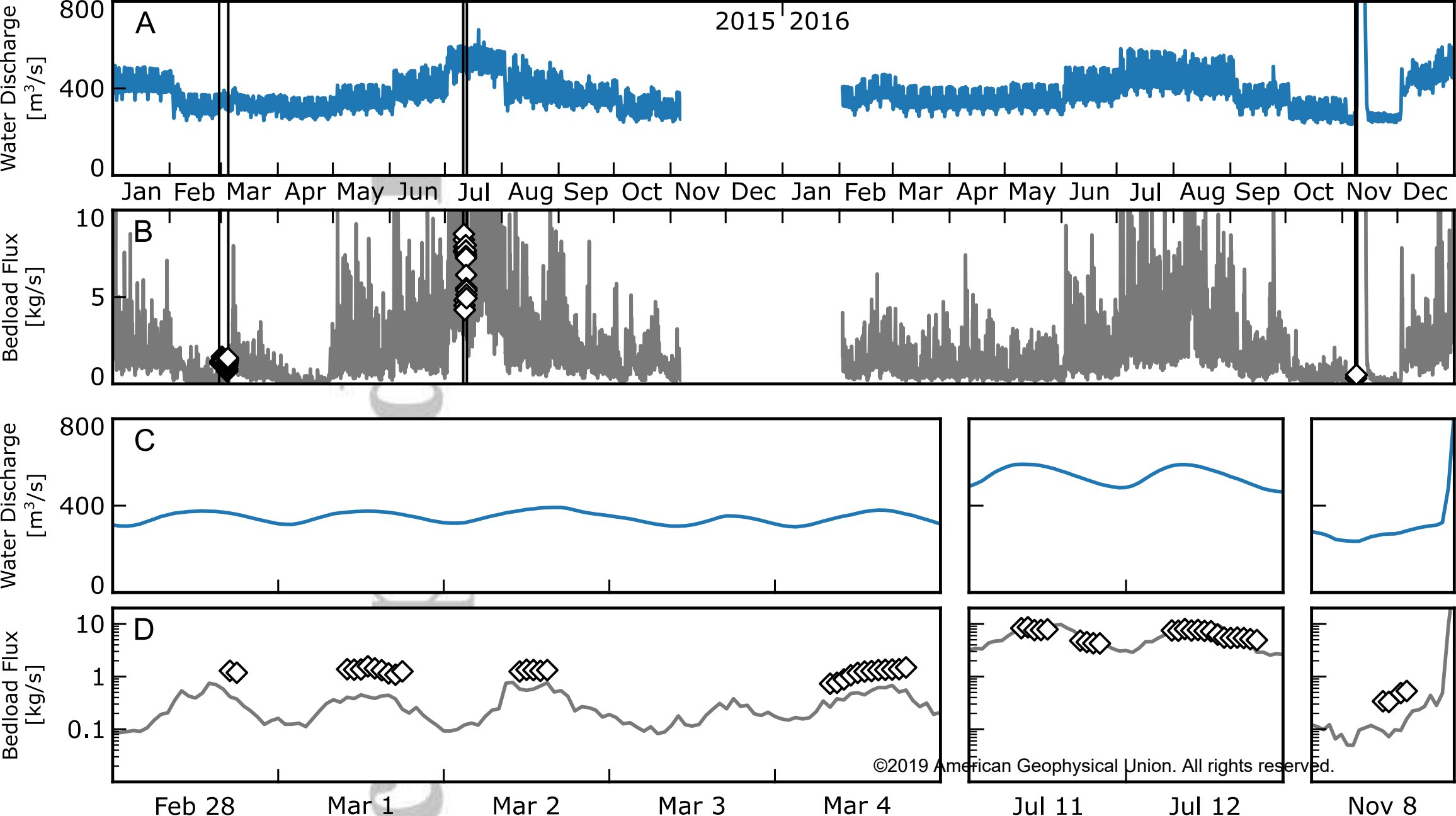
0  
0

100 m

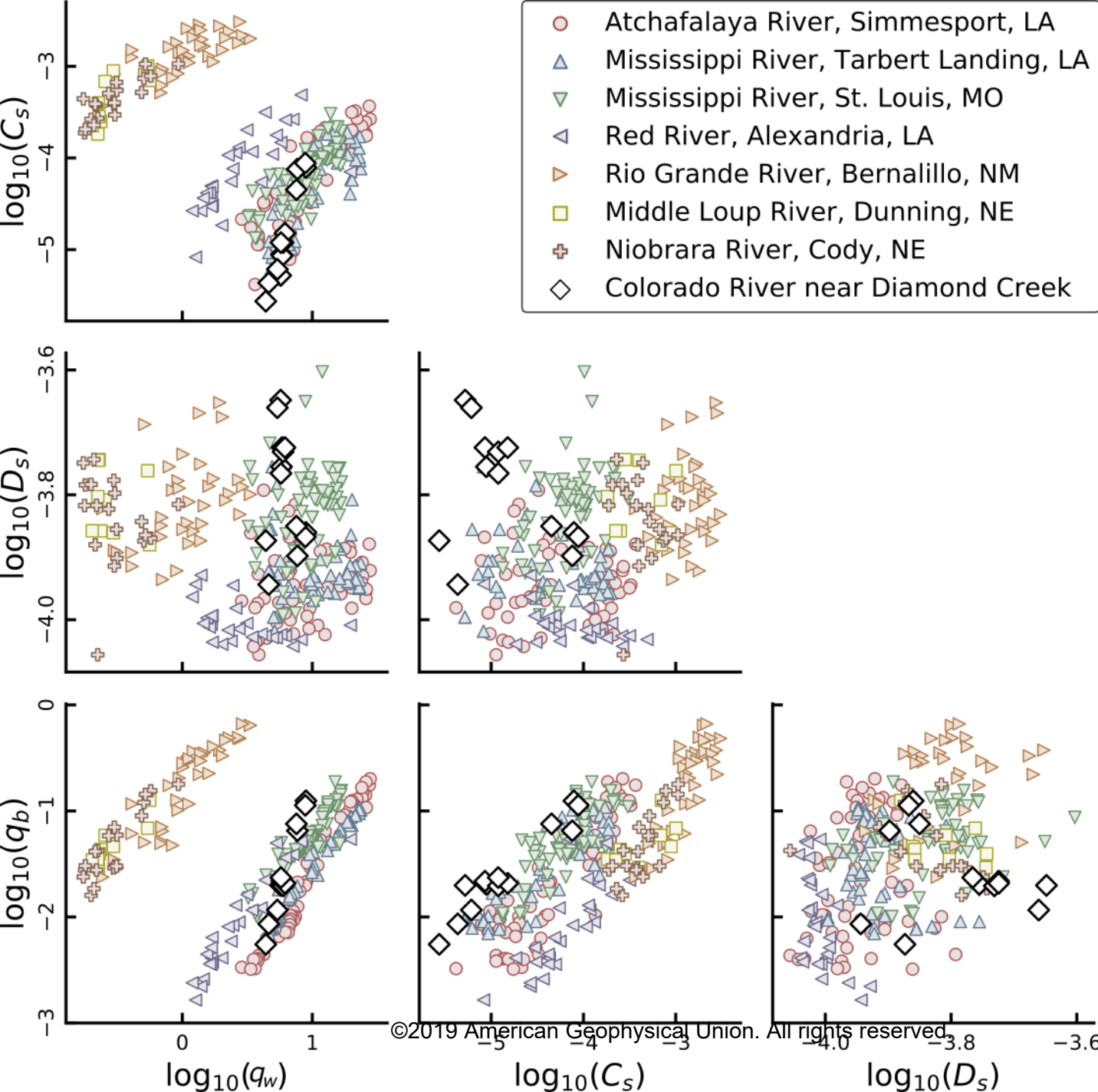
©2019 American Geophysical Union. All rights reserved.

500 ft

# Accepted Article

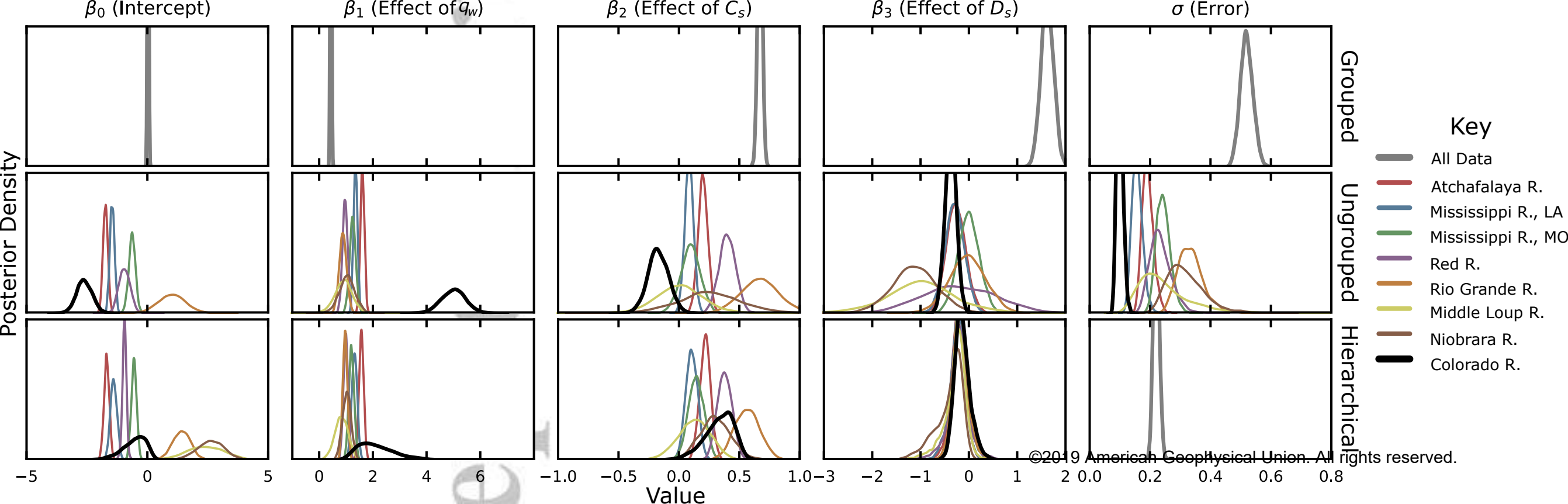


# Accepted Article

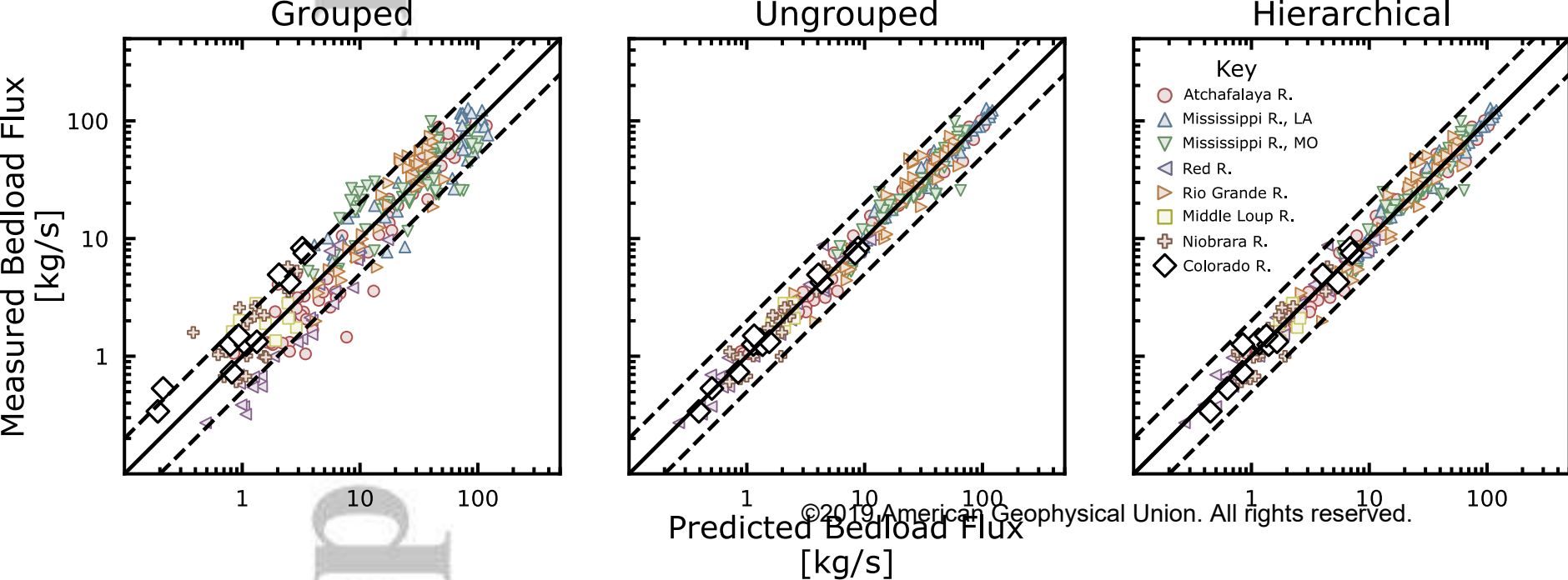


# Accepted Article

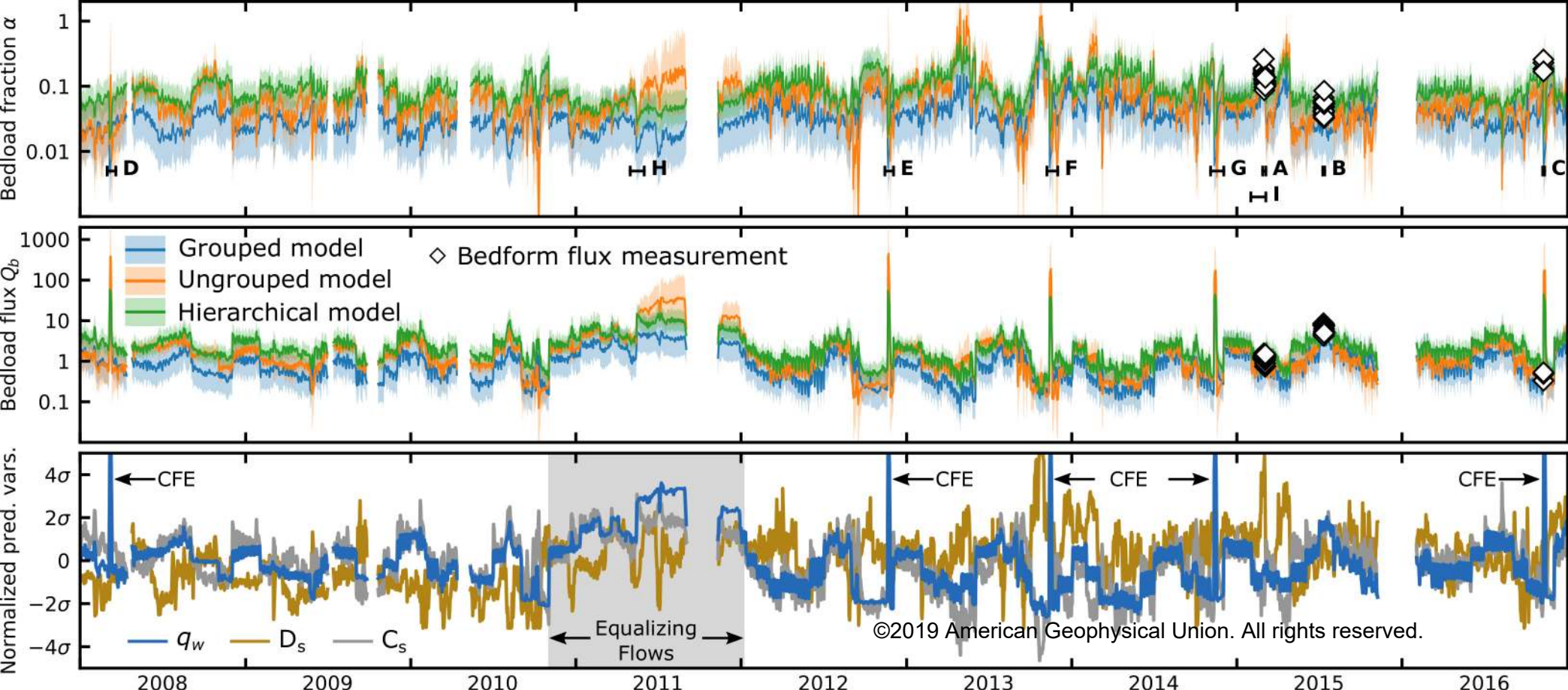
Posterior Density



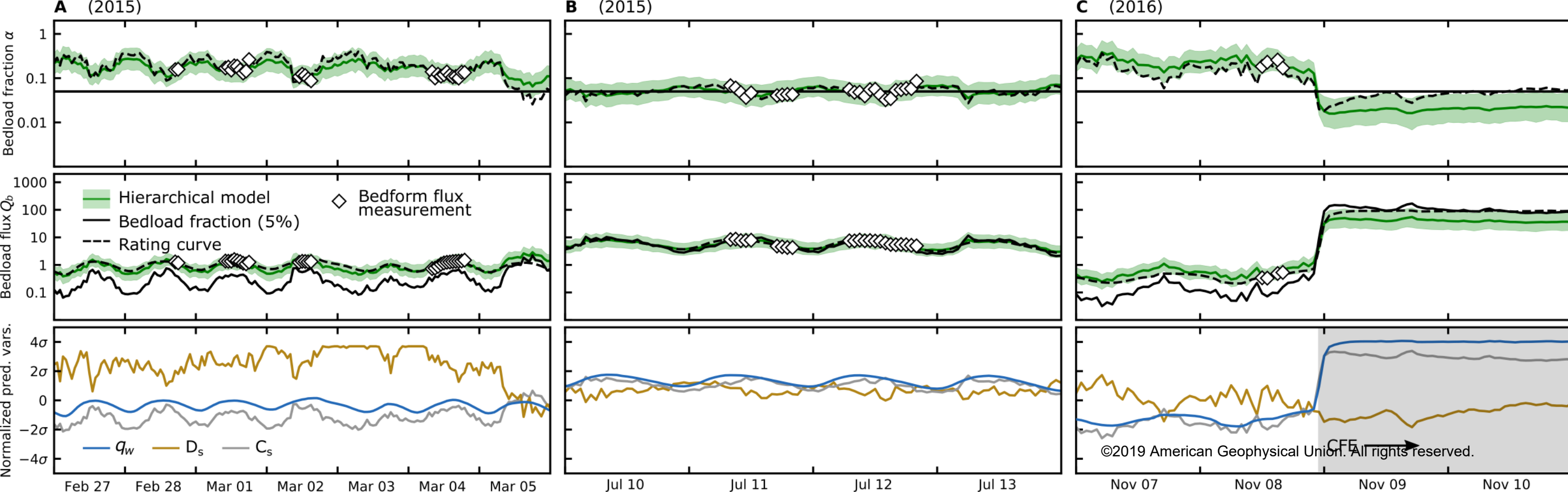
# Accepted Article



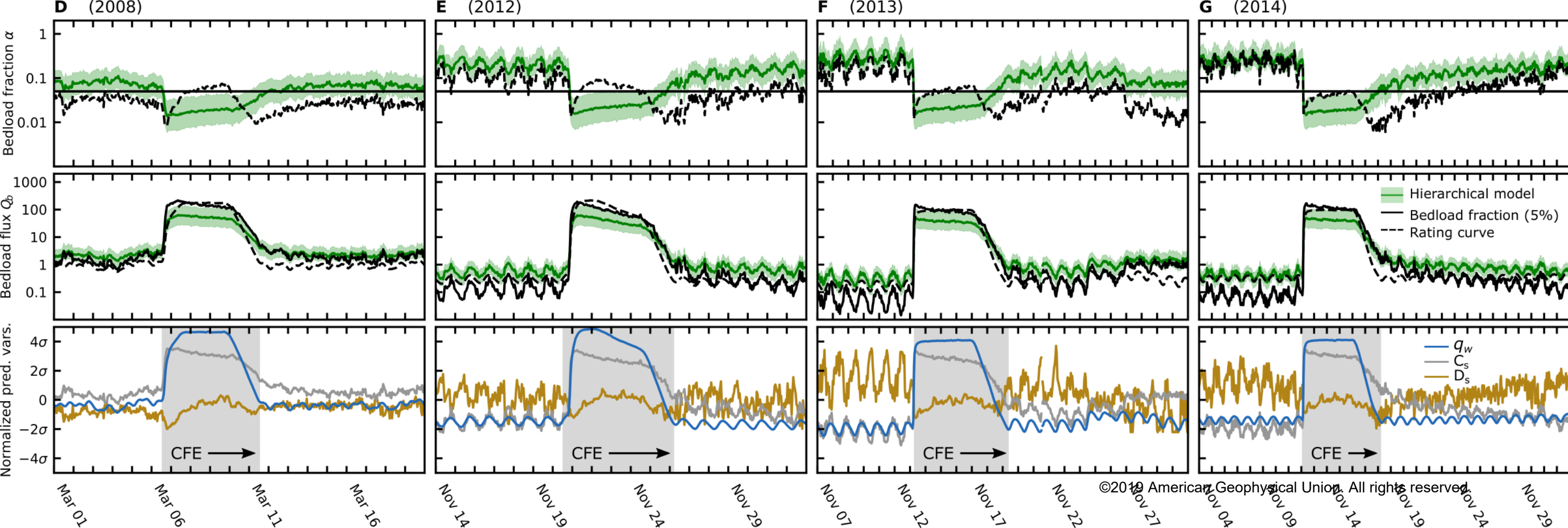
# Accepted Article



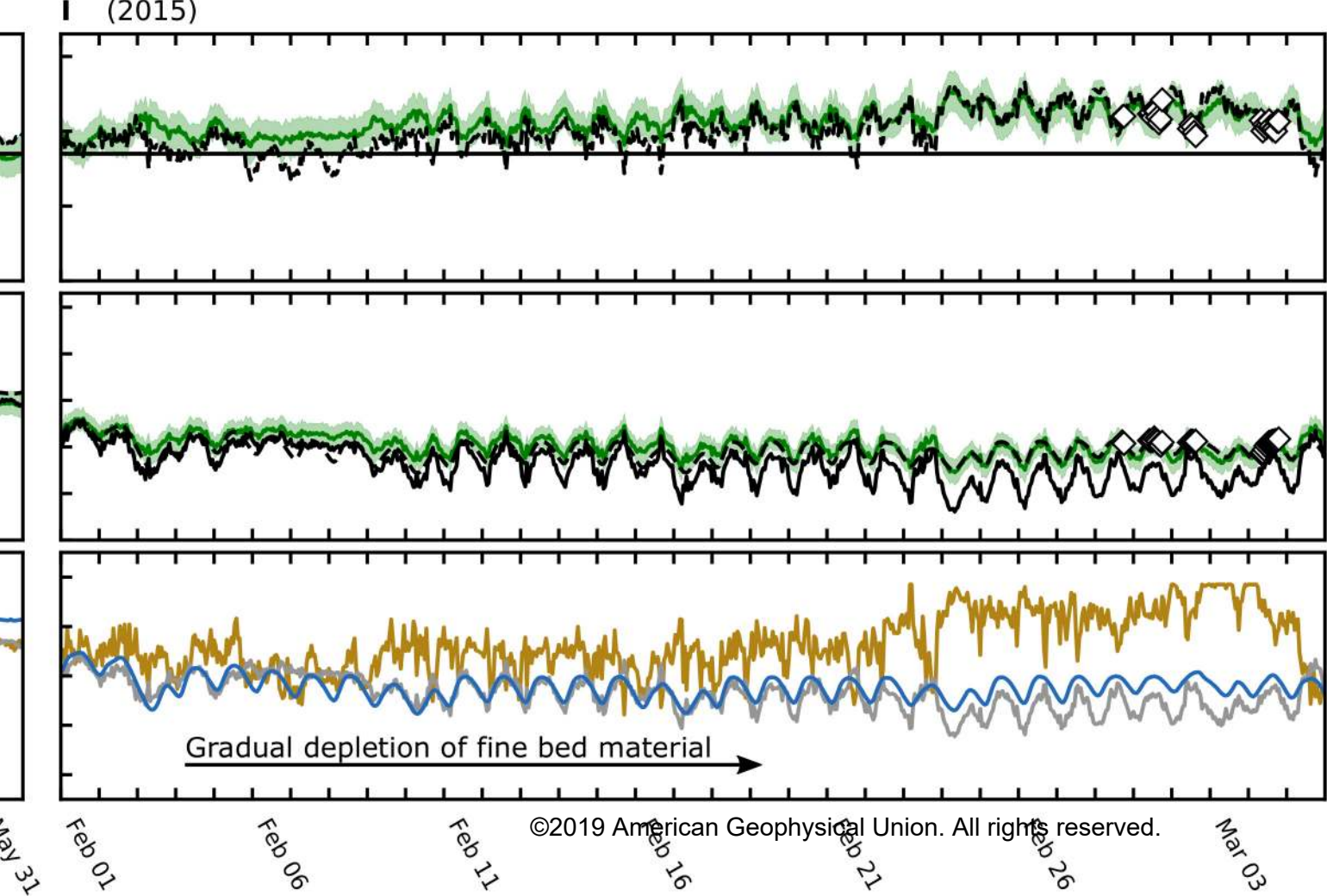
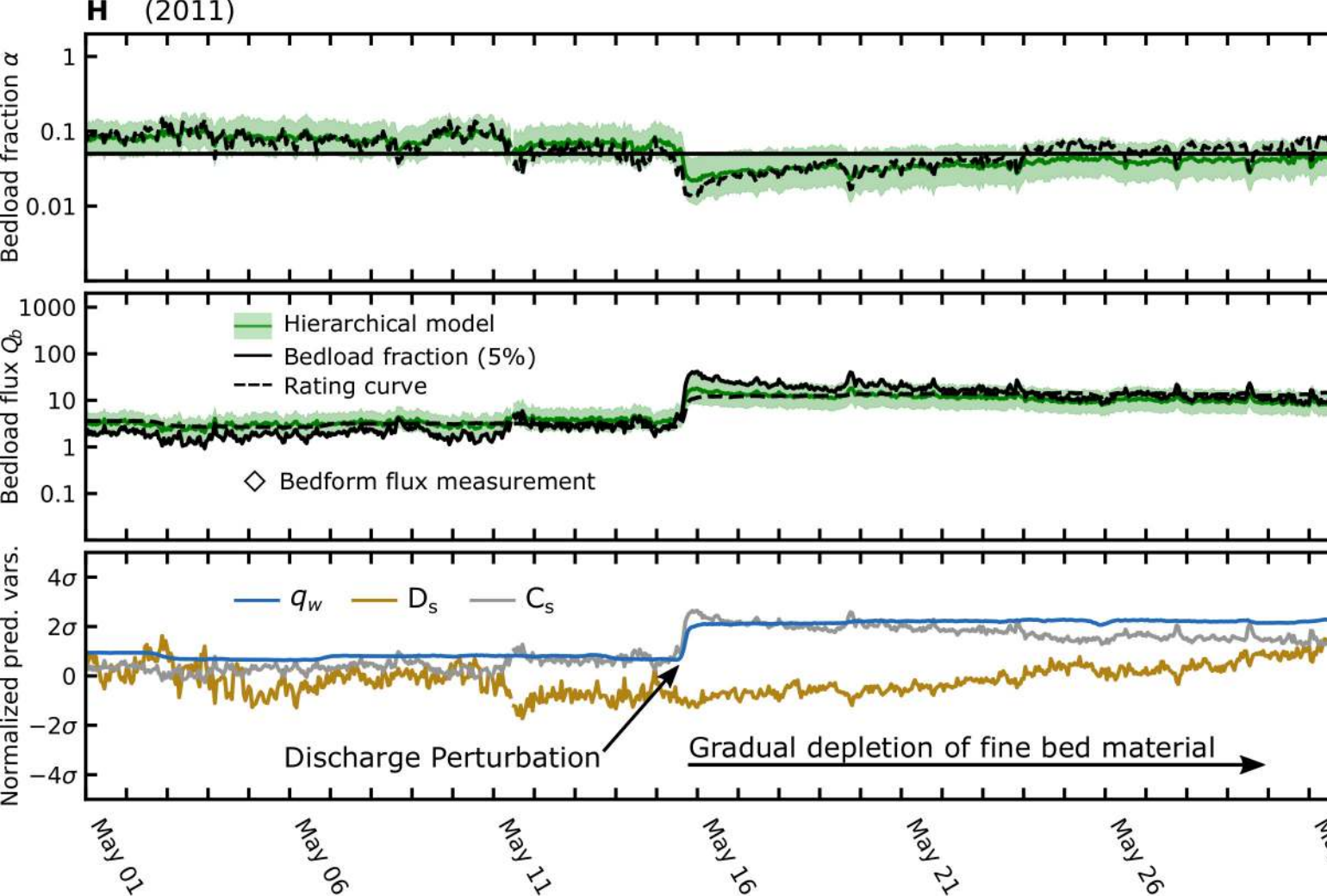
# Accepted Article



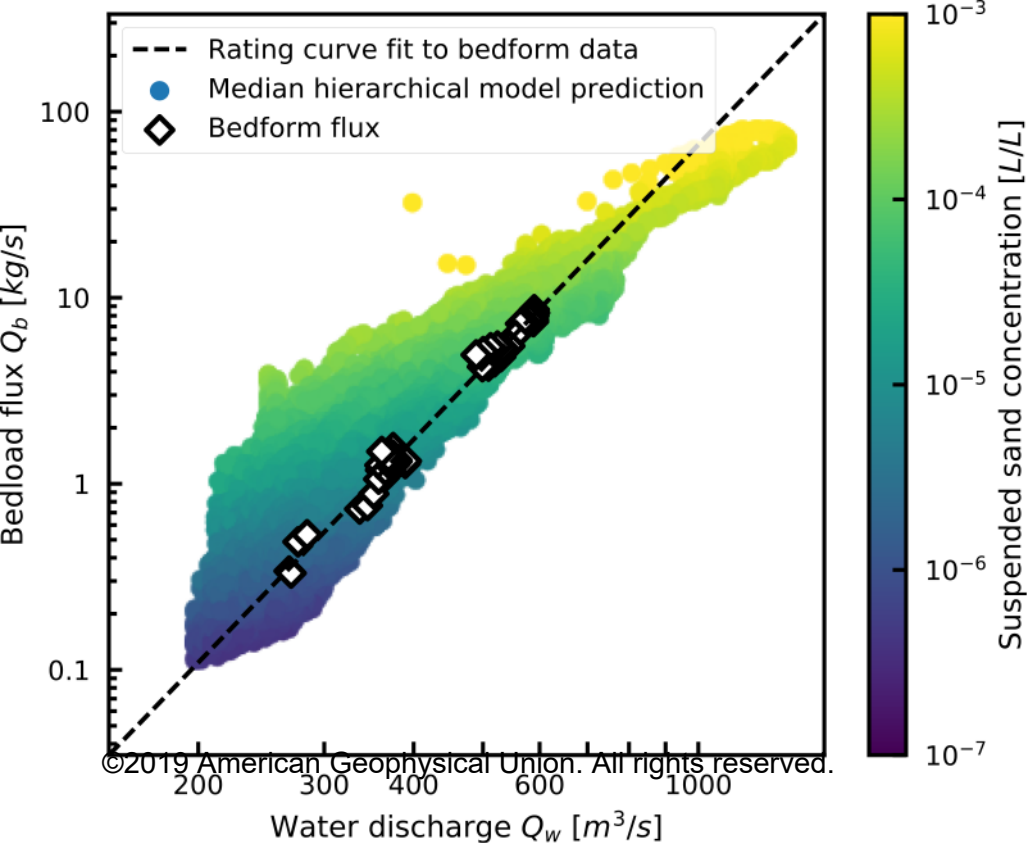
# Accepted Article



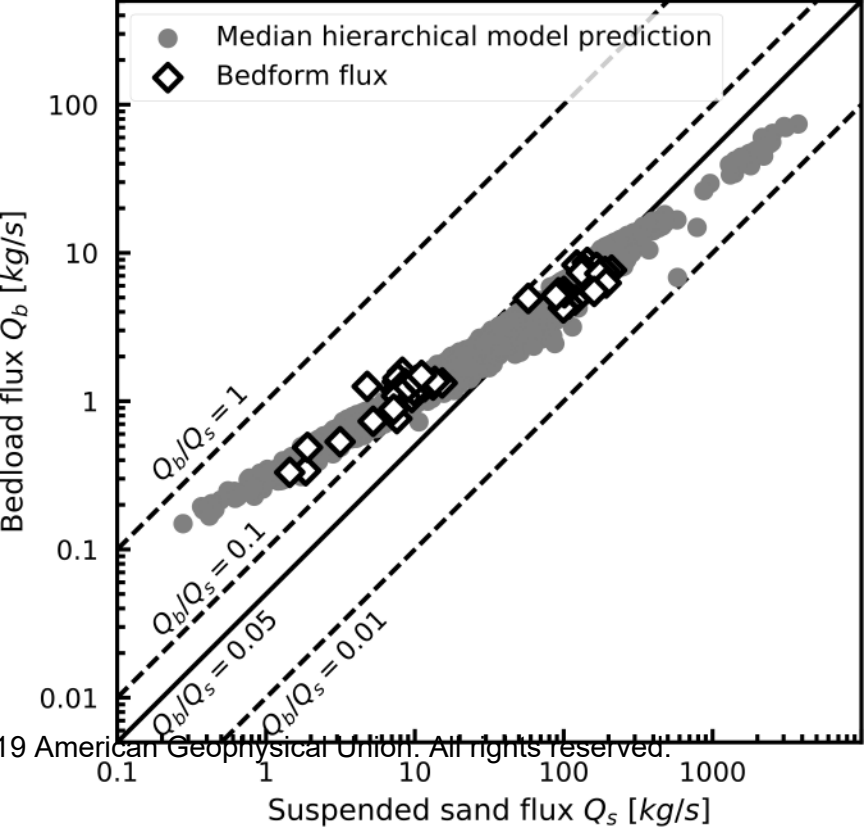
# Accepted Article



# Accepted Article



# Accepted Article



# Accepted Article

